

NASA/17-

206053

Final
10/30/97
OC/T
12/8

FINAL REPORT ON


**NUMERICAL STUDY OF MAGNETIC DAMPING DURING
UNIDIRECTIONAL SOLIDIFICATION
(NASA GRANT #: NCC3-435)**

Duration: October 1, 1995 - September 30, 1997

Submitted to:
H. C. de Groh III
Processing Sciences and Technology Branch
NASA Lewis Research Center, M.S. 105-1
Cleveland, OH 44135

Submitted by:

Principal Investigator:
Dr. Ben Q. Li

Signature: 
Associate Professor of Mechanical Engineering
School of Mechanical & Materials Engineering
Washington State University
Pullman, WA 99164-2920
Phone: 509-335-7386
Fax: 509-335-4662

October 30, 1997

TABLE OF CONTENTS

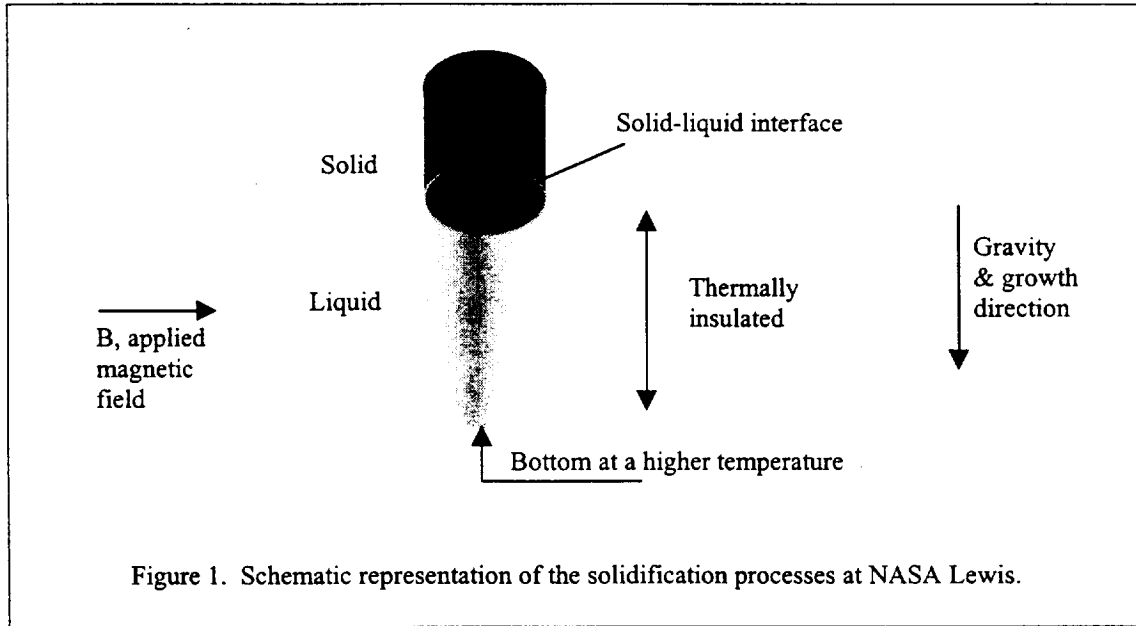
EXECUTIVE SUMMARY	1
1. INTRODUCTION	2
2. THE 3-D FINITE ELEMENT MODEL	3
3. NUMERICAL RESULTS AND FINDINGS	4
(a) Test against published results for known conditions	4
(b) Melt convection in the cylindrical cavity without imposed magnetic field	5
(c) Magnetic damping effects on the melt flow in the cavity	5
(d) Research findings that are different than those reported	6
(e) Some unresolved issues that require further studies	7
4. CONCLUDING REMARKS	7
5. BIBLIOGRAPHY	8
APPEDIX I: PROBLEM STATEMENT	9
APPENDIX II: FINITE ELEMENT FORMULATION	13
TABLES	17
FIGURES	21

EXECUTIVE SUMMARY

A fully 3-D numerical model is developed to represent magnetic damping of complex fluid flow, heat transfer and electromagnetic field distributions in a melt cavity. The model is developed based on our in-house finite element code for the fluid flow, heat transfer and electromagnetic field calculations. The computer code has been tested against benchmark test problems that are solved by other commercial codes as well as analytical solutions whenever available. The numerical model is tested against numerical and experimental results for water reported in literature. With the model so tested, various numerical simulations are carried out for the Sn-35.5% Pb melt convection and temperature distribution in a cylindrical cavity with and without the presence of a transverse magnetic field. Numerical results show that magnetic damping can be effectively applied to reduce turbulence and flow levels in the melt undergoing solidification and over a certain threshold value a higher magnetic field resulted in a higher velocity reduction. It is found also that for a fully 3-D representation of the magnetic damping effects, the electric field induced in the melt by the applied DC magnetic field does not vanish, as some researchers suggested, and must be included even for molten metal and semiconductors. Also, for the study of the melt flow instability, a long enough time has to be applied to ensure the final fluid flow recirculation pattern. Moreover, our numerical results suggested that there seems to exist a threshold value of applied magnetic field, above which magnetic damping becomes possible and below which the convection in the melt is actually enhanced. Because of the limited financial resource allocated for the project, we are unable to carry out extensive study on this effect, which should warrant further theoretical and experimental study. In that endeavor, the developed numerical model should be very useful; and the model should serve as a useful tool for exploring necessary design parameters for planning magnetic damping experiments and interpreting the experimental results.

1. INTRODUCTION

Recently, NASA Lewis has conducted a set of Sn-Pb alloy solidification experiments in High Temperature Directional Solidification Furnace under the influence of a transverse magnetic field to investigate magnetic damping effects (Song, Tewari and de Groh, 1996). The schematical representation of their system is sketched below in Figure 1.



With the experimental setup, they studied fluid flow, thermal transport and macrosegregation during solidification of Pb-Sn alloys with and without an externally imposed horizontal magnetic field. Temperature fluctuations were observed in the liquid pool during the solidification processes. It was found that these thermal fluctuations evolve from none to cyclic to time periodic having multiharmonics and finally to random as the Rayleigh number of the system increases. The application of the magnetic field decreases convection level in the liquid pool, but even high magnetic field (0.45 T) was unable to eliminate the convection. Application of the magnetic fields also resulted in changing temperature fluctuations from sinusoidal to pulsed wave behavior. These experimental measurements are very useful for providing first hand evidence on the effectiveness of magnetic damping. However, accompanying theoretical analyses are needed to determine quantitatively how the thermal field is affected by a magnetically damped fluid flow field during solidification.

The objective of this small grant is to initiate the development of first principle mathematical models for magnetically damped fluid flow and heat transfer in solidifying liquids. Our intention is two fold: (1) to acquire a basic understanding of magnetically damped flow phenomena in the aforementioned system by studying a simplified system such as a 3-D cylindrical cavity without considering the complex phase change phenomena associated with solidification; and (2) to establish a capability for 3-D simulation of magnetically damped flows with which further studies on magnetic damping effects on melt flow and solidification processes can be conducted. Following this direction, we have developed a full 3-D finite element model, based on our in-house fluid flow and heat transfer and electromagnetic model capabilities, for magnetic damping of fluid flow and thermal phenomena in a 3-D cylindrical cavity. The

diameter of the cavity is the same as used in the Lewis experiments (Song *et al.*, 1996), but the length is varied to simulate the different stages of solidification. Sn-Pb melt is used and the properties of the melt are provided by H. C. de Groh at NASA Lewis, along with other operating parameters. Both pseudo steady state and transient numerical models were developed. Some simulations were conducted with the model developed to both demonstrate the capability of the model and also to gain some basic understanding of magnetic damping effect during melt processing of relevance to NASA Lewis experiments. The modeling strategy, numerical results and findings and the future directions on the work are described below.

2. THE 3-D FINITE ELEMENT MODEL

The mathematical formulation of the magnetic damped fluid flow and heat transfer problem is given in Appendix I. Because of the limited funds available, we focus our attention on the model capability development and basic understanding, rather than a comprehensive study, of the magnetic damping effects on fluid flow and heat transfer phenomena in the Sn-Pb melts during solidification. Thus, we consider natural convection and magnetic damping phenomena in a 3-D cylindrical cavity with its side thermally insulated and top and bottom surfaces fixed at lower and high temperatures. Solidification and other complicating factors such as crystal growth rate, etc., are not considered in the model to simplify the calculations.

Originally the models were planned to be developed using FIDAP, a commercial finite element code for flow and thermal computations, and simulations were to be carried out using the Supercomputers at the University of Illinois. However, two difficulties encountered during the course of the model development with FIDAP. First several testing runs with FIDAP for flows without applied magnetic fields were made on the Supercomputer and it was found that it took too long to obtain the results. The major time was spent on waiting and queue list, even though the highest priority was employed. For example, for a 3-D mesh of $12 \times 5 \times 10$ 8-node elements used for the simulation of natural convection in a cylinder of our interest, one transient run that requires about 200 time steps took about 4 CPU hours; but the real turnout time was about 4 to 5 days, because of the heavy usage of the machine. Second, some time during the model development when we carefully studied FIDAP's formulation of magnetic damping problems as stated in their manual (p. 2-32, FIDAP Theoretical Manual), we found that the current density resulting from the interaction of the magnetic field with the fluid flow field seems to be calculated incorrectly. Since the source code is not available, we were not able to confirm whether this is a typographical error or the code calculates the problem as stated (usually it does and should also). Because of the limited computing sites where FIDAP is available and because there is potentially an error in their problem formulation, we started to develop our own 3-D finite element code for the planned numerical modeling effort. Fortunately, at that time, our 2-D finite element model was completed and was in use for g-jitter induced fluid flow, heat and mass transfer calculations. Our 3-D code development was then just an extension of the 2-D finite element code. The finite element formulation of the magnetic damping problems based on which our code was developed is provided in Appendix II. The development of our own code entailed program coding, debugging and extensive testing of the code against analytical solutions and calculations from other codes such as FIDAP and FLOW3D for benchmark type problems. Some of testing has been discussed in one of our recent publications (Pan, Li and deGroh, 1997).

It should be noted that having our own code gives us tremendous flexibility, although the development process itself is a bit painful in that various cases, including those not of direct interest to our model development, must be examined to ensure the correctness of the code. With our own code, we now are able to load the program onto any platforms we can get an access to and thus many computational cases can be run simultaneously to increase the computational efficiency. Many calculations were carried out on the LSU IBM-6000 RISC cluster machines, where several runs can be made simultaneously.

In Fall 1997, the PI left LSU to join the School of Mechanical and Materials Engineering at Washington State University. The model was imported from Louisiana State University to Washington State University and additional cases were run on an Onix machine, which is capable of supercomputing. For the results presented below, a typical run of 2000 time steps leading to a steady state would take 20 CPU hours for a mesh size of $17 \times 6 \times 10$ 8-node elements on the Onix machine. This change in environment required re-setting up the local computing environment for the PI's laboratory, including purchase of PCs, printers and tuning software, etc., which are required for printing out the calculated results and preparing this report.

3. NUMERICAL RESULTS AND FINDINGS

The developed numerical model is used to carry out simulations for magnetically damped flows in Sn-Pb melts for various operating conditions. The parameters for the calculations are given in Tables 1 and 2. To test the mesh dependency of our calculations, numerical experiments were carried out using different mesh sizes or different number of elements. Basically, different meshes were used until the results no longer show the mesh dependency. The mesh, as shown in Figure A2, is the one of the meshes used for the calculations for cavities with small h/d ratio. More meshes are placed in the vertical direction when a larger h/d ratio cavity is considered. Unless stated otherwise, all the calculations for magnetic damping assumed that the magnetic field is applied in the x-direction (see Figure A1). For the results presented in the figures below, the time and velocity are normalized by the time factor (τ) and the velocity factor (u_0) given in Table 2 and Rayleigh numbers and other conditions are based on the stability diagram given by Muller (1988).

(a) Test against published results for known conditions

Before reporting the results on Sn-35.5% Pb melt flows, we would like to discuss some of testing cases with water for which published work is available. Muller's research group had published results on flow instability of water in a cylinder heated from below for various aspect ratios and also conducted experiments to verify their calculations (Muller *et al.*, 1984). Figures 2 and 3 depict the comparison between our computed results and the results from a finite difference model and corresponding water model developed by Muller's group. The parameters used for the calculations are given in Table 3. It is clear that for both symmetric and un-symmetric flow patterns the results computed from our 3-D finite element model compared very well with those reported by Muller's group, indicating that our numerical model can provide reasonably good prediction of fluid flow and heat transfer behavior of the fluids in the geometry under consideration.

(b) Melt convection in the cylindrical cavity without imposed magnetic field

Figures 4-6 show the evolution of the temperature and fluid flow fields for the Sn-35.5% Pb melt in the cylindrical cavity of $h/d=0.5$. Both 3-D and 2-D views (plane views) are presented. Note that the contour levels in Figure 4 correspond to those marked in Figure 6. It is apparent that both the fluid flow and temperature fields evolve starting from some arbitrary temperature pulse and eventually arrive at a steady state after 2000 time steps (corresponding to the real time of 3.05 seconds and dimensionless $t=2.0$). At the final steady state, a symmetric pattern is obtained with the flow moving downward at the center and upward from the side wall. It should be stressed that for such an unstable case a final stage of the flow pattern is strongly affected by the initial temperature pulse to induce the flow. When an appropriate temperature pulse is used, a flow pattern opposite to what is shown is also possible. This has been reported for water case and confirmed by our study as well (see Figure 2 above).

The transient melt flow and temperature distribution for the Sn-35.5% Pb melt in a cavity of $h/d=1$ is shown in Figures 7-9. In this case, a non-symmetric flow pattern is developed in the cylinder (see Figures 7(d), 8(d) and 9(g) and (h), which is caused by the non-symmetric pulse (see Figure 7(a)). Again, a long simulation time (time step=2000) is required to reach the steady state, afterwards the fields values are no longer changing.

Similar transient calculations were also carried out for the melt column with a higher aspect ratio, $h/d=3$. The final steady state results are given in Figure 10. Clearly, the strong flow is developed near the bottom which is fixed at a higher temperature. The flow pattern is non-symmetric and the flow has a strong effect on the temperature field there as well. In the upper portion of the melt pool, the fluid is basically quiescent.

(c) Magnetic damping effects on the melt flow in the cavity

Figures 11-13 shows the transient development of the fluid flow and temperature distributions in the Sn-35.5% Pb melt in the cavity of $h/d=0.5$ with an applied magnetic field ($B=0.05$ T), with other conditions kept the same as those in Figure 4-6. Comparison of Figs 11-13 with Figs 4-6 clearly indicates the magnetic damping effects. In particular, when the system reaches the steady state, the fluid flow level is damped very substantially and temperature profile is basically flat. Note also that the steady state is reached within about 800 time steps.

The magnetic damping effect on the melt flow in the Sn-35.5% Pb melt with an aspect ratio of $h/d=1$ is shown in Figures 14 and 15. Apparently, with an increase in the applied magnetic field strength, magnetic damping becomes more effective, as expected. Figure 16 shows the numerical results obtained for magnetic damping of melt flow in the Sn-35.5% Pb melt with an aspect ratio of $h/d=3$ in a transverse magnetic field ($B=0.05$ T), where it can be seen that the applied magnetic field results in the reduction of the melt flow in the liquid pool. However, in comparison with Figure 10, the temperature field does not seem to change greatly.

The higher magnetic field effect on the fluid flow and temperature distributions in the Sn-35.5% Pb melt for 3 different aspect ratios ($h/d=0.5$, $h/d=1$ and $h/d=3$) is illustrated in Figures 17-19, where $B=0.5$ T. Clearly, for all the cases, the damping effects are sufficiently strong that the temperature distribution in the system is basically controlled by diffusion, as is evident by the parallel temperature profiles in these figures.

One of the important reasons for applying the magnetic damping is to reduce the possible melt flow turbulence during solidification. The current model should help to provide some insight into the effectiveness of magnetic damping effects on the melt flow turbulence in the system. Figure 20 compares the effect of the different magnetic field strengths as applied to damp the turbulence in the system (with $h/d=1$, $Ra=8 \times 10^5$). Inspection of the plots in the figure indicates that in the absence of the magnetic field ($B=0$) and with a small magnetic field present ($B=0.005$ T), the flow remains turbulent. With a higher magnetic field ($B=0.05$ T), the turbulence is substantially reduced and melt flows in the laminar region. With an even higher magnetic field ($B=0.5$ T), the turbulence is further reduced (the non-dimensionalized U_{max} is reduced to 1.57 from 172.5). Note that the velocity is plotted with the same magnitude scale for all the plots in Figure 20; the temperature contour clearly illustrates the effects of the melt flow still present in the system.

Besides the results reported here, additional runs were made to investigate the effect of the direction of the applied magnetic field on the fluid flow and heat transfer effects. Results show that the magnetic field, when applied in the transverse direction provides the most effective damping effects. For symmetric flow pattern, the x- and y-direction magnetic field seems to produce similar results. For a non-symmetric flow pattern, the damping effect is stronger when the magnetic field is applied at the plane in which flow circulation is strongest.

(d) Research findings that are different than those reported

Our numerical simulations unveiled two important points that are either unclear in the literature or reported differently. For the Sn-35.5% Pb case of $h/d=0.5$, we found that calculations have to proceed for longer time than 600 (dimensionless) used by Muller's group in order to resolve the ordered pattern. Figure 21 shows the evolution of the fluid flow and temperature profiles for the Sn-35.5% Pb melt at various time steps. According to Muller's numerical study of molten melts with similar properties in which numerical simulations were carried out up to 600 time steps (undimensionalized the same as this study) (Muller, 1988), no symmetric flow pattern would exist for this condition. Our results compare well with theirs up to the time they terminated their calculations (time step=600) (Figure 21(a) shows the flow field at time step=500). However, the flow is actually still evolving and a longer run time is needed for this case to reach a steady state, as clearly indicated by the plotted results. For this particular case under consideration, the steady state is attained at about time step=2000 and by then a symmetric pattern is attained. It is noted here that Muller's work might have used a different starting pulse because his flow pattern is just opposite to that reported here; nonetheless a steady state of symmetric pattern should prevail if a long run time is used.

Another important finding resulted from this study, but unclear or misleading in the literature, is that for 3-D magnetic damping modeling studies, the induced electric field must be included in the current density and hence the Lorentz force calculations. Muller's group recently did some 3-D simulations for semiconductor melt but without considering the electric field effect (Baumgartl *et al.*, 1990). They argued, based on the cited references, that the conductivity of the molten metal and semiconductor is high and therefore the electric field is zero everywhere. Our study indicated that these references dealt with either 2-D or axi-symmetric case with a special arrangement of the magnetic field and for these special cases one can approve that the induced electric field is indeed zero everywhere in the melt. This approval, however, can not be

generalized to a fully 3-dimensional case. Indeed, our numerical calculations showed that for a fully 3-D model the induced electric field is not zero everywhere and hence must be included in the damping force calculations. Some of these calculated results are given in Figure 22.

(e) Some unresolved issues that require further studies

From our limited numerical experiments, we also found that a pure application of magnetic field does not necessarily decrease the fluid flow, as one would normally expect from simple Hartmann flow studies. On contrary, a DC magnetic field may actually *enhance* the liquid convection in melts when a weak magnetic field is applied. A set of these results is given in Figure 23. There it is clear that with $B=0.005T$, the flow velocity is actually increased and damping effects are not obvious until the applied magnetic field is about $0.016 T$. This phenomenon seems to occur in all other cases we tested. Our studies indicate that this flow augmentation seems to be dependent on the combination of the Rayleigh number of the system and the strength of the applied magnetic field. In essence, there seems to exist a magnetic field strength threshold above which the magnetic field acts to reduce the convection and below which the applied field actually enhances the convection. Our limited numerical experiments seem to suggest that in general a higher threshold value is needed for a higher Rayleigh number. Because of the limited time and resource allocated for this project, we were unable to quantify the effect in this report and also the possible effect of the other system parameters such as aspect ratios on the threshold value to obtain magnetic damping effect. This should be a very important issue that requires further study, considering the widespread use of magnetic damping in solidification processes.

4. CONCLUDING REMARKS

A fully 3-D numerical model was developed to represent magnetic damping of complex fluid flow, heat transfer and electromagnetic field distributions in a cylindrical melt cavity. The model was developed based on our in-house finite element code for the fluid flow, heat transfer and electromagnetic field calculations, which has been tested against benchmark test problems that are solved by other commercial codes as well as analytical solutions when available. The numerical model was tested against available numerical and experimental results reported for water. With the model so tested, various numerical simulations were carried out for the Sn-35.5% Pb melt. Numerical results showed that magnetic damping can be effectively applied to reduce turbulence and flow levels in the melt undergoing solidification and over a certain threshold value a higher magnetic field resulted in higher velocity reduction. It is found also that for a fully 3-D representation of the magnetic damping effects, the induced electric field in the melt does not vanish, as some researchers suggested, and must in general be included even for highly conducting melts such as molten metal and semiconductors. Also, for the study of the melt flow instability, a long enough simulation time has to be applied to ensure the final fluid flow circulation pattern. Moreover, our numerical results suggested that there seems to exist a threshold value of applied magnetic field above which magnetic damping becomes possible and below which the convection in the melt is actually enhanced. Because of the limited financial resource allocated for the project, we were unable to carry out extensive study on this effect, which should warrant further theoretical and experimental study. In conclusion, the numerical model developed in this study may now be used to study the fundamentals governing the magnetic damping phenomena in the solidifying melts and should serve as a useful tool for exploring necessary design parameters magnetic damping experiments.

5. BIBLIOGRAPHY

Baumgartl, J., Gewald, M., Rupp, R., Stierlen, J. and Muller, G. (1990). The use of the magnetic fields and microgravity in melt growth of semiconductors: a comparative study. in *Proceedings of VIth Euro. Symp. on Materials and Fluids Sciences in Microgravity*, Oxford, UK, Jan, 1990, p. 47.

Muller, G., G. Neumann, G. and Weber, W. (1984). Numerical convection in vertical Bridgman Configurations. *J. Crystal Growth* **70** (1984) 78-93

Muller, G. (1988). *Convection and inhomogeneities in crystal growth from the melt*. Springer-Verlag, Berlin.

Pan, B. Li, B. Q. and de Groh, H. C. (1997). Finite element study of magnetic damping of g-jitter driven flows in microgravity. *Spacebound-97*, Montreal, Ca, May, 1997, to appear.

Song, H, Tewari, S. N. and de Groh III, H. C. (1996) Convection during thermally unstable solidification of Pb-Sn in a magnetic field. *Metal. Trans.*, **27A**, 1095-1110

APPEDIX I: PROBLEM STATEMENT

To simplify the calculations, magnetic field damping effects on the fluid flow in a 3-D cylindrical cavity as shown in Figure A1, instead of the whole solidification process as appears in Figure 1, are considered.

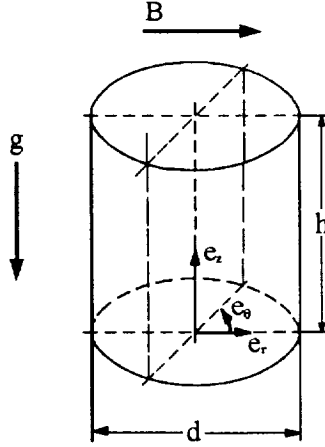


Figure A1. Schematic representation of the 3-D model for magnetic damping studies.

The mathematical equations governing the fluid flow, temperature distribution and electromagnetic field distributions in the melt, along with appropriate boundary conditions, are written as follows.

GOVERNING EQUATIONS

Continuity Equation:

$$\nabla \cdot \mathbf{u} = 0 \quad (1)$$

Momentum Equation:

$$\rho \left(\frac{\partial \mathbf{u}}{\partial t} + \mathbf{u} \cdot \nabla \mathbf{u} \right) = -\nabla p + \mu \nabla^2 \mathbf{u} - \rho g \beta_t (T - T_0) + \sigma_m (\mathbf{E} + \mathbf{u} \times \mathbf{B}) \times \mathbf{B} \quad (2)$$

Energy Equation:

$$\rho c_p \left(\frac{\partial T}{\partial t} + \mathbf{u} \cdot \nabla T \right) = k \nabla^2 T \quad (3)$$

Electromagnetic Field Equation:

$$\mathbf{J} = \sigma_m (\mathbf{E} + \mathbf{u} \times \mathbf{B}) \quad (4)$$

$$\nabla \cdot \mathbf{J} = 0 \quad (5)$$

$$\nabla \times \mathbf{E} = 0 \quad (6)$$

$$\mathbf{E} = -\nabla \Phi \quad (7)$$

$$\nabla^2 \Phi = \nabla \cdot (\mathbf{B} \times \mathbf{u}) = \mathbf{B} \cdot (\nabla \times \mathbf{u}) \quad (8)$$

Thus for the problem under consideration, the Maxwell equations reduces to one equation for an unknown electric potential, that is, Eq. (8), and other relevant quantities can be calculated once the potential is known. This simplification comes from the fact that for metallic liquid, the induced magnetic field \mathbf{b} is proportional to the magnetic Reynolds number and that the magnetic Reynolds number is much smaller than imposed magnetic field \mathbf{B}_0 , thereby $\mathbf{B} = \mathbf{B}_0$. This curl free field allows us to write \mathbf{E} as the gradient of an electric potential Φ . This, combined with the fact that the current density is a divergence free field, results in $\nabla^2 \Phi = \mathbf{B} \cdot (\nabla \times \mathbf{u})$.

The boundary conditions for the problem represent the physical constraints needed to solve the problem. For the present problem, the no slip conditions are applied at the solid walls, side walls are thermally insulated, the top and bottom walls are at the fixed temperatures and the electric current density is zero on the solid walls as no current can escape from the system, because the walls are electrically insulated as well. Mathematically, these conditions are given as follows.

$$\text{Side Walls:} \quad \frac{\partial T}{\partial n} = 0 \quad \mathbf{u} = 0 \quad \frac{\partial \Phi}{\partial n} = 0$$

$$\text{Top Wall:} \quad T = T_L \quad \mathbf{u} = 0 \quad \frac{\partial \Phi}{\partial n} = 0$$

$$\text{Bottom Wall:} \quad T = T_H \quad \mathbf{u} = 0 \quad \frac{\partial \Phi}{\partial n} = 0$$

To facilitate numerical computations, it is more convenient to non-dimensionalize the above equations and boundary conditions. To do that, we use the standard velocity, time, and length scales for natural convection in enclosures [1] and define the following dimensionless variables,

$$\begin{aligned}\mathbf{u}^* &= u h / \alpha & \mathbf{x}^* &= \mathbf{x} / h & t^* &= t \alpha / h^2 \\ p^* &= p h^2 / \rho \alpha^2 & T^* &= (T - T_L) / (T_H - T_L) \\ \mathbf{B}^* &= \mathbf{B} / B_0 & \Phi^* &= \Phi / \alpha B_0 & E^* &= E h / \alpha B_0 & J^* &= J h / \sigma_m \alpha B_0\end{aligned}$$

With the above definitions, the governing equations and the boundary conditions may be re-written in non-dimensional forms,

Continuity Equation:

$$\nabla^* \cdot \mathbf{u}^* = 0 \quad (9)$$

Momentum Equation:

$$\frac{\partial \mathbf{u}^*}{\partial t^*} + \mathbf{u}^* \cdot \nabla^* \mathbf{u}^* = -\nabla^* p^* + Pr \nabla^{*2} \mathbf{u}^* - Ra Pr T^* \mathbf{e}_z + Ha^2 Pr (-\nabla^* \Phi^* + \mathbf{u}^* \times \mathbf{B}^*) \times \mathbf{B}^* \quad (10)$$

Energy Equation:

$$\frac{\partial T^*}{\partial t^*} + \mathbf{u}^* \cdot \nabla^* T^* = \nabla^{*2} T^* \quad (11)$$

Electromagnetic Field Equation:

$$\nabla^{*2} \Phi^* = \nabla \cdot (\mathbf{B}^* \times \mathbf{u}^*) = \mathbf{B}^* \cdot (\nabla^* \times \mathbf{u}^*) \quad (12)$$

Boundary conditions

Side Walls: $\frac{\partial T^*}{\partial n} = 0$ $\mathbf{u}^* = 0$ $\frac{\partial \Phi^*}{\partial n} = 0$

Top Wall: $T^* = 0$ $\mathbf{u}^* = 0$ $\frac{\partial \Phi^*}{\partial n} = 0$

Bottom Wall: $T^* = 1$ $\mathbf{u}^* = 0$ $\frac{\partial \Phi^*}{\partial n} = 0$

The non-dimensionalization process often gives rise to a set of dimensionless parameters that characterize the performance of the system under study. For our problems, these parameters are given in the following table.

DIMENSIONLESS SYSTEM PARAMETERS

Dimensionless Number	Definition
Rayleigh number	$Ra = \frac{\beta g (T_H - T_L) h^3}{\nu \alpha}$
Prandtl number	$Pr = \frac{\nu}{\alpha}$
Hartman number	$Ha = B_0 h \sqrt{\frac{\sigma_m}{\mu}}$
Thermal Diffusivity	$\alpha = \frac{k}{\rho c_p}$
Kinematic Viscosity	$\nu = \frac{\mu}{\rho}$

APPENDIX II: FINITE ELEMENT FORMULATION

1. Discretization and Interpolation:

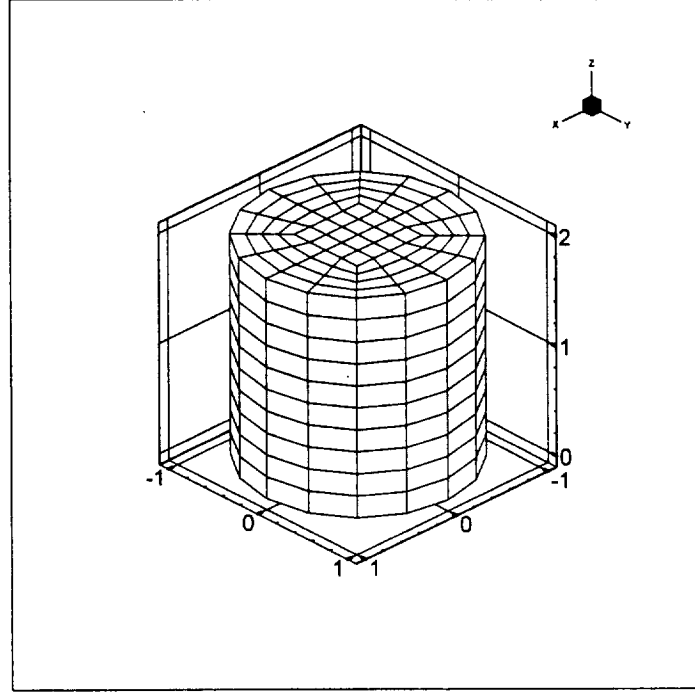


Figure A2. Finite element discretization of the 3-D cavity for magnetic damping of fluid flow studies.

We started with discretizing the domain into a finite number of elements as shown in Figure A2. Over each element, the dependent variables \mathbf{u} , T and Φ are interpolated by their nodal point values and the shape functions of $\phi(x_i)$ and for P we use $\psi(x_i)$ as the interpolation functions. Then the velocity, pressure, temperature and electric potential fields are approximated by:

$$\mathbf{u}_j(x_i, t) = \phi^T \mathbf{U}_j(t) \quad (13)$$

$$P(x_i, t) = \psi^T \mathbf{P}(t) \quad (14)$$

$$T(x_i, t) = \phi^T \mathbf{T}(t) \quad (15)$$

$$\Phi(x_i, t) = \phi^T \Phi(t) \quad i, j = 1, 2, 3 \quad (16)$$

where \mathbf{U}_j , \mathbf{P} , \mathbf{T} and Φ are vectors of approximate values of element nodal points.

Our calculations employ 8-node elements, as shown in Figure A3. The interpolation functions expressed in local coordinate are given by:

$$\phi = \{N_j, N_j, \dots, N_j, \dots\}^T ; \psi = 1 \quad (17)$$

$$N_j = \frac{1}{8}(1 + \xi\xi_j)(1 + \eta\eta_j) + (1 + \zeta\zeta_j) \quad (18)$$

where $\xi_j, \eta_j, \zeta_j = \pm 1$, $j = 1, 2, 3, \dots, 8$. Note that ψ is chosen one order lower than the interpolation function for the velocity field to satisfy the Babuška-Brezzi stability condition.

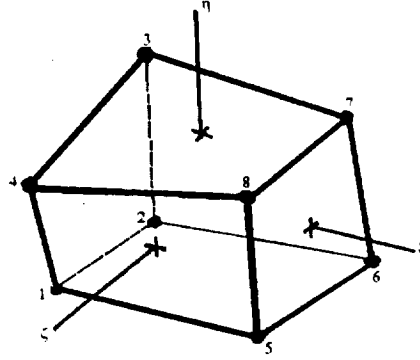


Figure A3. 8-node element in local coordinate system.

The interpolated velocity and other field variables can not satisfy the governing equations exactly. Substituting the interpolation equations into the governing equations, we get the residual functions R_1 , R_2 , R_3 and R_4 , which respectively represent error functions of the momentum, mass conservation, energy and electric potential equations. To simplify the calculations, the pressure may be treated using the penalty method, by which the penalty form of the continuity equation becomes,

$$P = -\frac{1}{\varepsilon} \nabla \cdot \mathbf{u} \quad (19)$$

where ε is the penalty parameter.

Substituting the interpolation functions into the governing equations, one has the following residual functions for the field variables,

$$\mathbf{f}_1(\phi, \psi, \mathbf{U}_i, \mathbf{P}, \mathbf{T}, \Phi) = \mathbf{R}_1 \quad \text{Momentum} \quad (20)$$

$$\mathbf{f}_2(\psi, \phi, \mathbf{U}_i, \mathbf{P}) = \mathbf{R}_2 \quad \text{Penalty Continuum} \quad (21)$$

$$\mathbf{f}_3(\phi, \mathbf{U}_i, \mathbf{T}) = \mathbf{R}_3 \quad \text{Energy} \quad (22)$$

$$\mathbf{f}_4(\phi, \mathbf{U}_i, \Phi) = \mathbf{R}_4 \quad \text{Electric Potential} \quad (23)$$

2. The Galerkin Weighted Residual Method:

Finite element formulation of nonlinear equations, as discussed in the present case, is carried out using the Galerkin Weighted Residual method. By this method, the residuals of the differential equations are made orthogonal to independent weighting functions, and these weighting functions are chosen to be the same as the shape functions for the unknowns:

$$\int R_2 \psi dV = 0 \quad (24)$$

$$\int R_i \phi dV = 0 \quad i = 1, 3, 4 \quad (25)$$

Applying the Green theorem to the above equations and carrying out involved algebraic operations, one has the following set of matrix equations for the unknowns defined at the nodal points,

$$\mathbf{M} \dot{\mathbf{U}} + \mathbf{K}(\mathbf{U})\mathbf{U} + \mathbf{C}_p \mathbf{P} + \mathbf{C}_B \mathbf{T} = \mathbf{F}(\mathbf{U}) \quad (26)$$

$$\mathbf{M}_T \dot{\mathbf{T}} + \mathbf{K}_T(\mathbf{U})\mathbf{T} = \mathbf{F}_T \quad (27)$$

$$-\varepsilon \mathbf{M}_p \mathbf{P} = \mathbf{C}_p^T \mathbf{U} \quad (28)$$

$$\mathbf{K}_\Phi \Phi + \mathbf{C}_\Phi \mathbf{U} = \mathbf{F}_\Phi \quad (29)$$

where now \mathbf{U} is a global vector containing all the nodal values of u , v and w . \mathbf{P} , \mathbf{T} and Φ are global pressure, temperature and electric potential vectors respectively. \mathbf{M} is the mass matrix, $\mathbf{K}(\mathbf{U}) = \mathbf{N}(\mathbf{U}) + \mathbf{K}_{\Phi\Phi} + \mathbf{K}_\mu$ is the stiffness matrix, where \mathbf{K}_μ is the viscous stiffness matrix, and $\mathbf{N}(\mathbf{U})$ is the advection stiffness matrix. \mathbf{C}_p is gradient matrix, \mathbf{K}_B the buoyancy matrix and $\mathbf{F}(\mathbf{U})$ the "force" vector which incorporates the Lorentz force term and the boundary conditions. In the temperature, penalty continuum and electric potential equations, the subscripts T , P and Φ refer to the corresponding sets of coefficients. Solving the pressure from continuity equation and substituting back into the momentum equation, one has the final form of the matrix representation of the governing equations in matrix form,

$$\begin{bmatrix} \mathbf{M} & 0 & 0 \\ 0 & \mathbf{M}_T & 0 \\ 0 & 0 & 0 \end{bmatrix} \begin{bmatrix} \dot{\mathbf{U}} \\ \dot{\mathbf{T}} \\ \dot{\Phi} \end{bmatrix} + \begin{bmatrix} \mathbf{K}(\mathbf{U}) - \mathbf{C}_p \mathbf{M}_p^{-1} \mathbf{C}_p^T & \mathbf{K}_B & 0 \\ 0 & \mathbf{K}_T & 0 \\ \mathbf{K}_\Phi & 0 & \mathbf{M}_\Phi \end{bmatrix} \begin{bmatrix} \mathbf{U} \\ \mathbf{T} \\ \Phi \end{bmatrix} = \begin{bmatrix} \mathbf{F}(\mathbf{U}) \\ \mathbf{F}_T \\ \mathbf{F}_\Phi \end{bmatrix} \quad (30)$$

where the coefficient matrices are defined by:

$$\mathbf{M} = \mathbf{M}_T = \int \phi \phi^T dV ; \quad \mathbf{M}_p = \int \psi \psi^T dV ; \quad \mathbf{K}_\mu = \int Pr \nabla \phi \bullet \nabla \phi^T dV$$

$$\mathbf{K}_T = \mathbf{K}_\phi = \int \nabla \phi \bullet \nabla \phi^T dV ; \quad \mathbf{N}(\mathbf{U}) = \mathbf{N}_T(\mathbf{U}) = \int \phi \mathbf{u} \bullet \nabla \phi^T dV$$

$$\mathbf{K}(\mathbf{U}) = \mathbf{N}(\mathbf{U}) + \mathbf{K}_{\phi\phi} + \mathbf{K}_\mu ; \quad \mathbf{K}_T(\mathbf{U}) = \mathbf{N}_T(\mathbf{U}) + \mathbf{K}_T$$

$$\mathbf{K}_{\phi\phi} = - \int \phi \mathbf{B} \times \mathbf{B} \times (\phi^T \hat{\mathbf{u}}) dV \text{ or } \mathbf{K}_{\phi\phi,ik} = - \int \phi \varepsilon_{ijk} \varepsilon_{jlm} B_l B_m \phi^T \hat{u}_k dV$$

$$\mathbf{C}_p = \int \phi (\nabla \psi^T) dV ; \quad \mathbf{C}_p^T = \int \psi (\nabla \phi^T) dV$$

$$\mathbf{K}_B = \int Ra Pr \mathbf{g} \phi \phi^T dV ; \quad \mathbf{K}_\phi = - \int \phi \mathbf{B} \bullet (\nabla \times \phi^T \hat{\mathbf{u}}) dV$$

$$\mathbf{F}(\mathbf{U}) = \{\mathbf{F}_1(\mathbf{U}), \mathbf{F}_2(\mathbf{U}), \mathbf{F}_3(\mathbf{U})\}^T ; \quad \mathbf{F}_j(\mathbf{U}) = - \int \sigma \phi dS + \int Ha^2 Pr (-\nabla \Phi \times \mathbf{B})_j dV$$

$$\mathbf{F}_T = - \int q_T \phi dS ; \quad \mathbf{F}_\phi = - \int q_E \phi dS$$

where \mathbf{K}_μ is the same for all 3 velocity components and \hat{u}_k refers to the kth component of the velocity.

The above matrix equations are solved using the successive substitution method and the time derivatives are approximated using the implicit finite difference scheme. Both variable time steps with automatic error tracking and time step automation and fixed time steps may be applied. The majority of the results presented in the report are calculated using the fixed time steps.

TABLES

Table 1: Parameters used for calculations

Parameter	Value
Diameter of cylinder (d)	7×10^{-3} m
Aspect ration (h/d)	0.5, 1.0, 3.0
Top wall temperature (T_L)	520 K
Magnetic field B_0	0.0~ 0.5 T
Gravity (g)	9.8 m s^{-2}

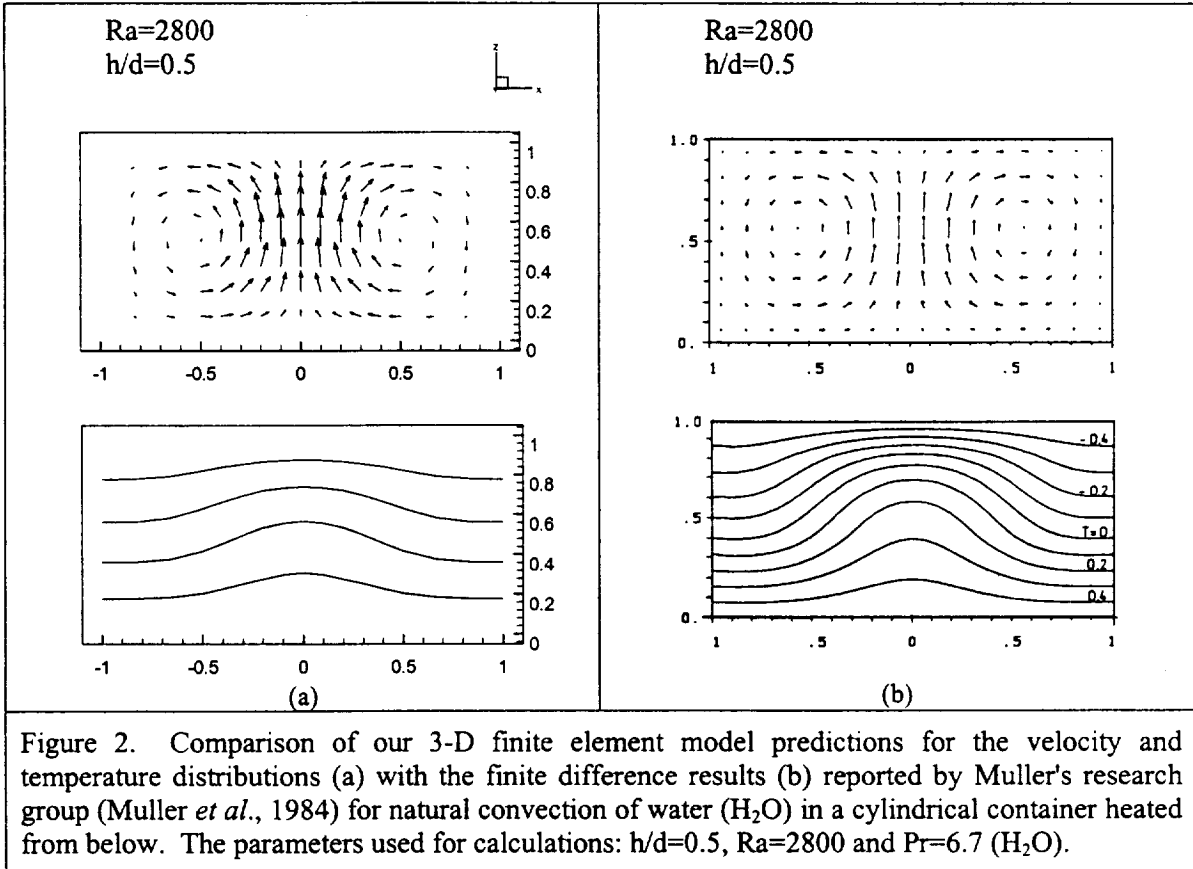
Table 2 Parameters of liquid metal used for calculations

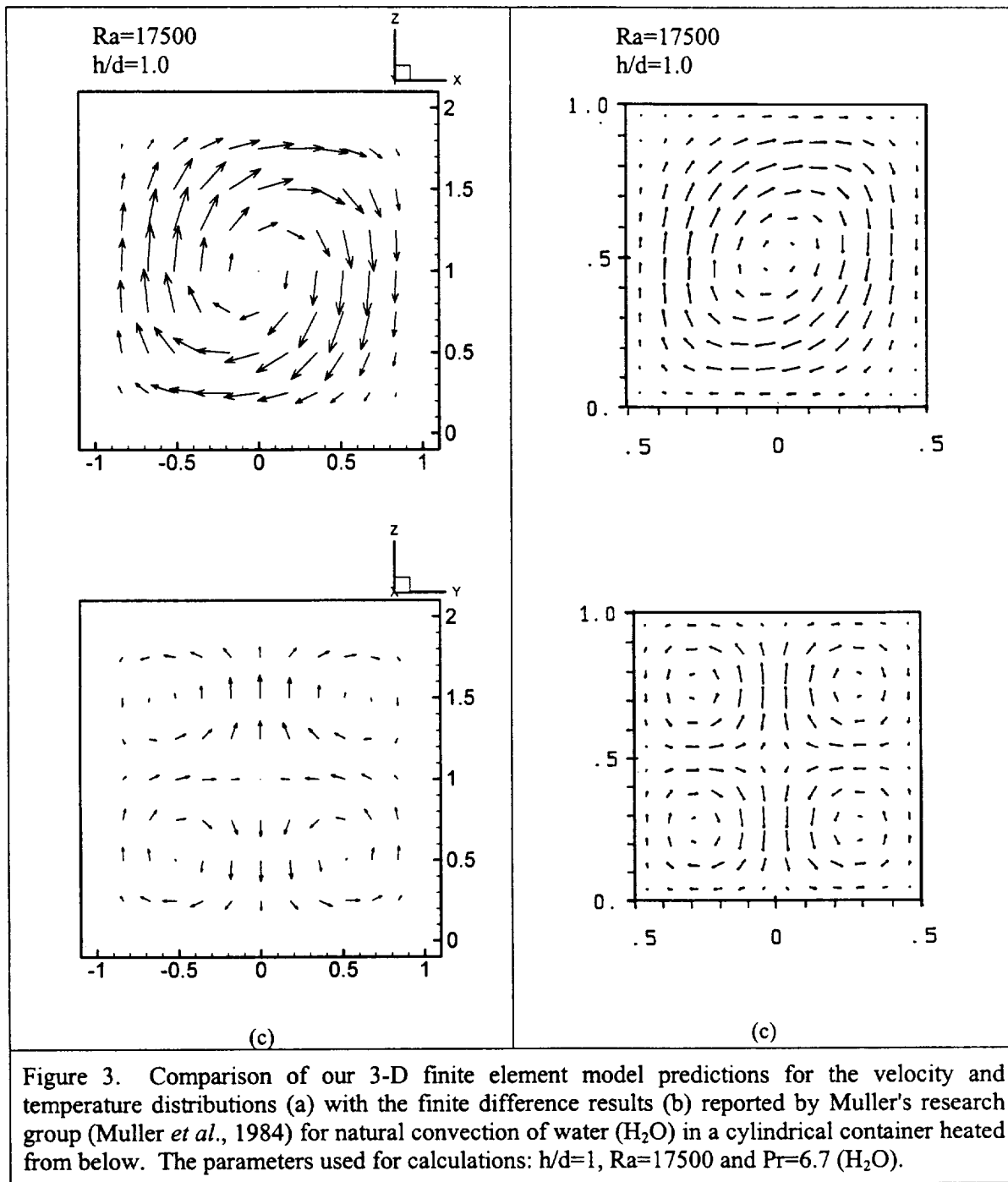
Property (Sn-35.5% Pb)	Value
Density of the melt (ρ)	$1.068 \times 10^4 \text{ kg m}^{-3}$
Thermal expansion coefficient (β)	$1.23 \times 10^{-4} \text{ K}^{-1}$
Thermal conductivity of the melt (k)	$14.9 \text{ W m}^{-1} \text{ K}^{-1}$
Specific Heat (C_p)	$173.70 \text{ J Kg}^{-1} \text{ K}^{-1}$
Viscosity of the melt (μ)	$2.410 \times 10^{-3} \text{ N s m}^{-2}$
Electronic conductivity of the melt (σ_m)	$3.402 \times 10^7 \Omega \text{ m}^{-1}$
Thermal diffusivity of the melt (α)	$8.032 \times 10^{-6} \text{ m}^2 \text{ s}^{-1}$
Kinematic viscosity of the melt (ν)	$2.257 \times 10^{-7} \text{ m}^2 \text{ s}^{-1}$
Associated dimensionless numbers	Value
Prandtl number (Pr)	0.0281
Rayleigh number (Ra)	$4.0 \times 10^3 \sim 8.0 \times 10^5$
Hartmann number (Ha)	0~1247.5
Time and velocity scales used to normalize the results presented in all the figures	Value
Time scale (τ)	1.53 (sec)
Velocity scale (u_0)	$2.29 \times 10^{-3} \text{ (m/s)}$

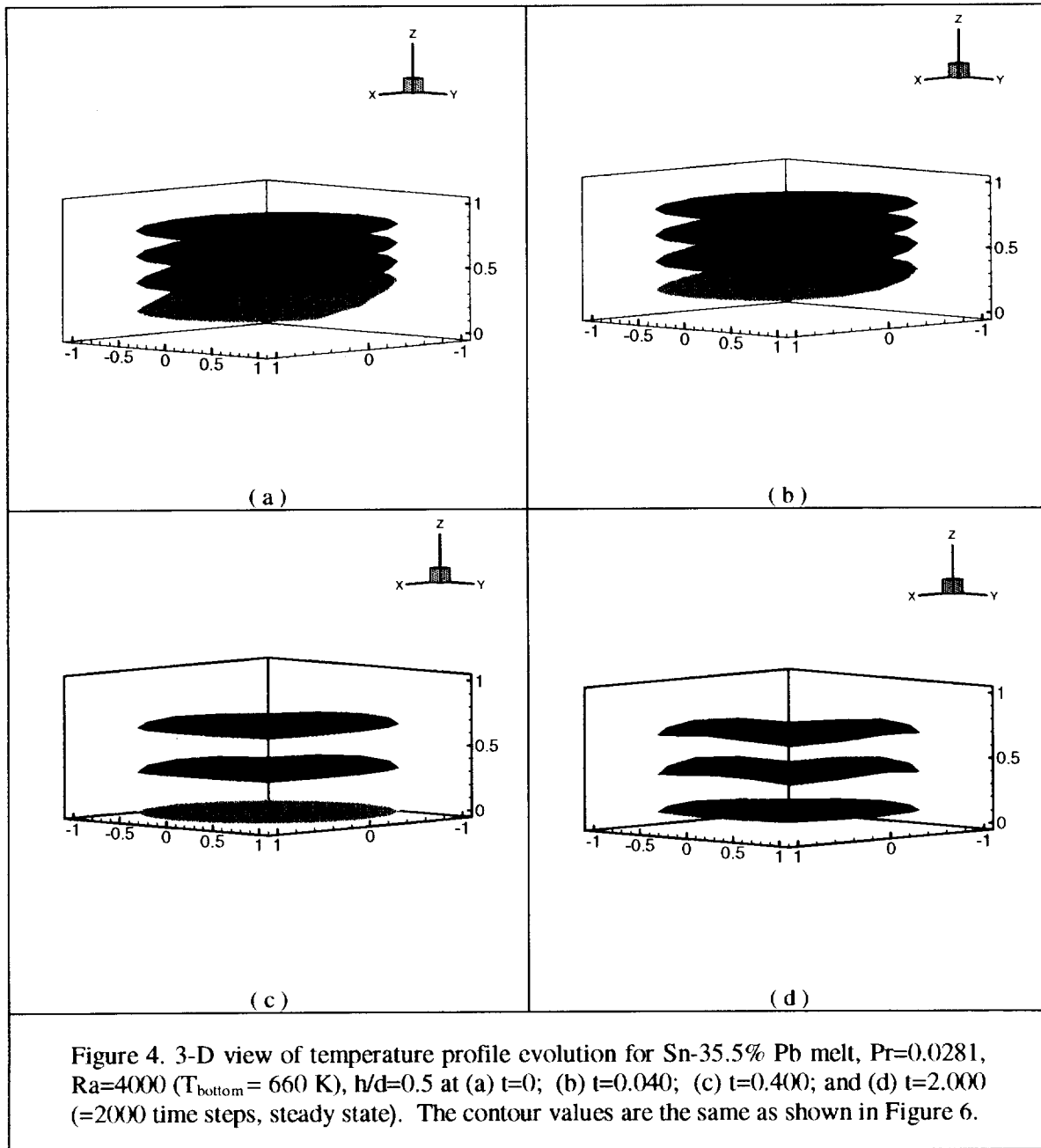
Table 3 Properties of water used for calculations

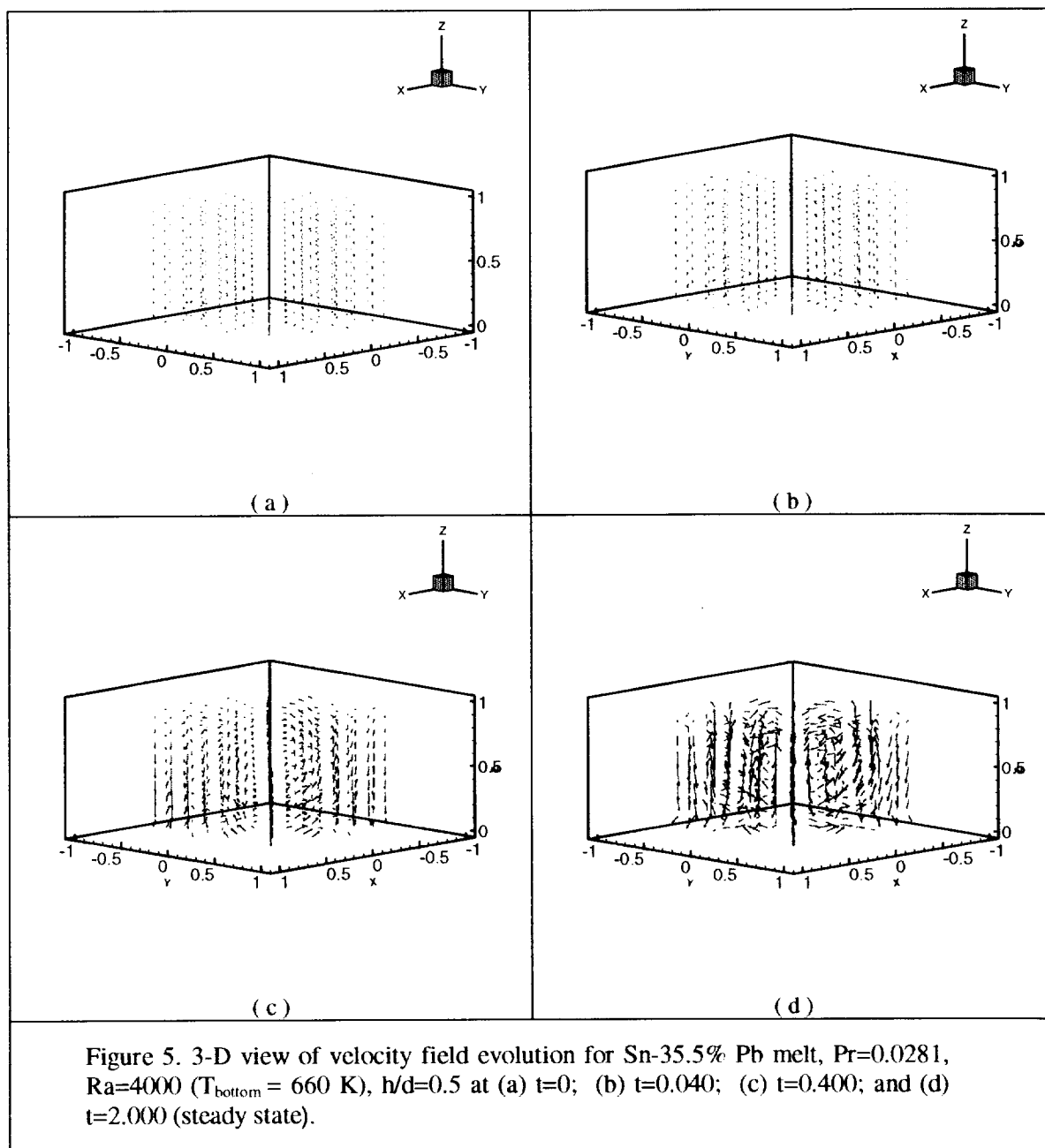
Property	Value
Thermal expansion coefficient (β)	$0.227 \times 10^{-3} \text{ K}^{-1}$
Thermal diffusivity of the melt (α)	$1.145 \times 10^{-7} \text{ m}^2 \text{ s}^{-1}$
Kinematic viscosity of the melt (ν)	$0.963 \times 10^{-6} \text{ m}^2 \text{ s}^{-1}$
Associated dimensionless numbers	Value
Prandtl number (Pr)	6.7
Rayleigh number (Ra)	$2.88 \times 10^3 \sim 1.0 \times 10^5$

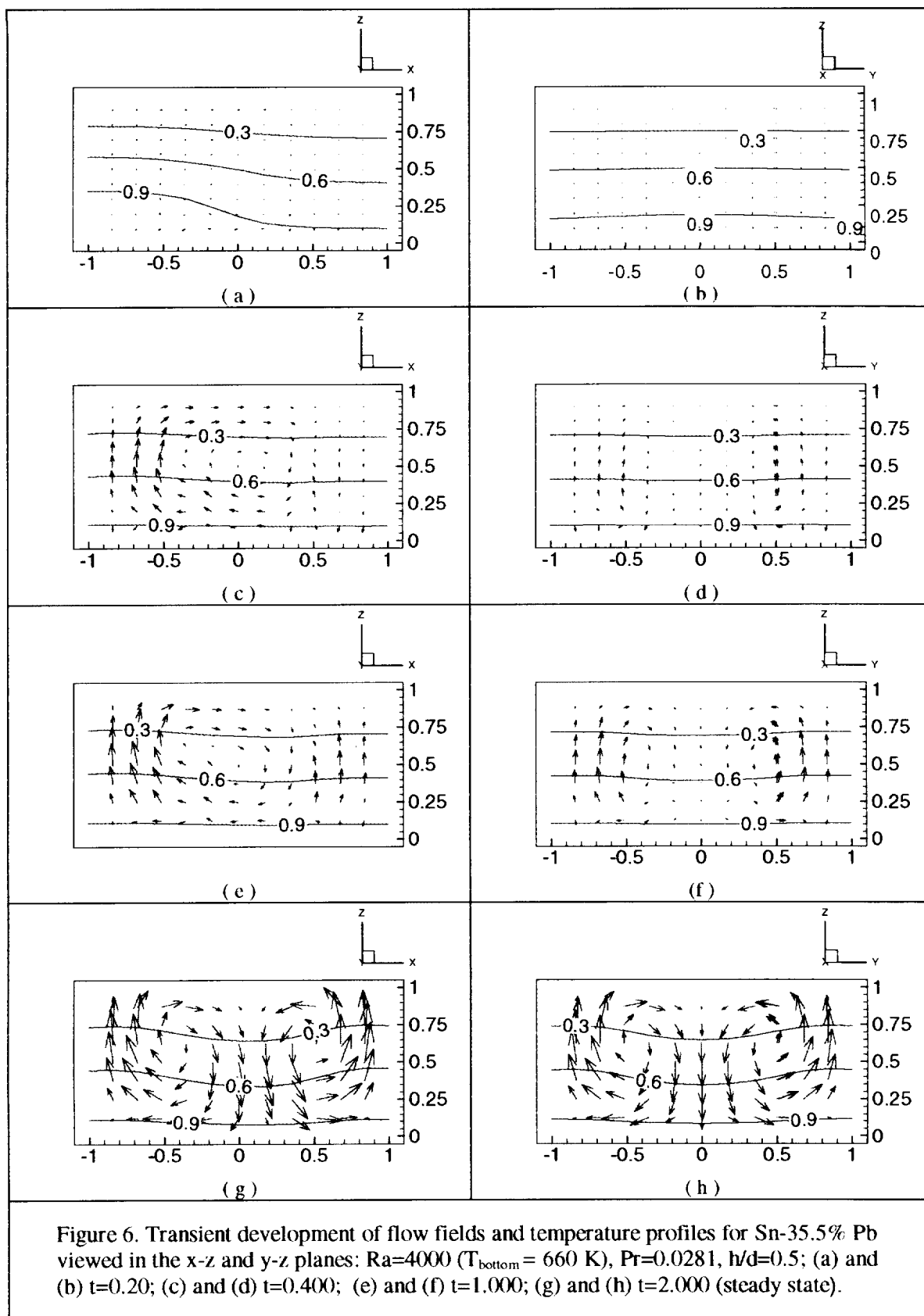
FIGURES

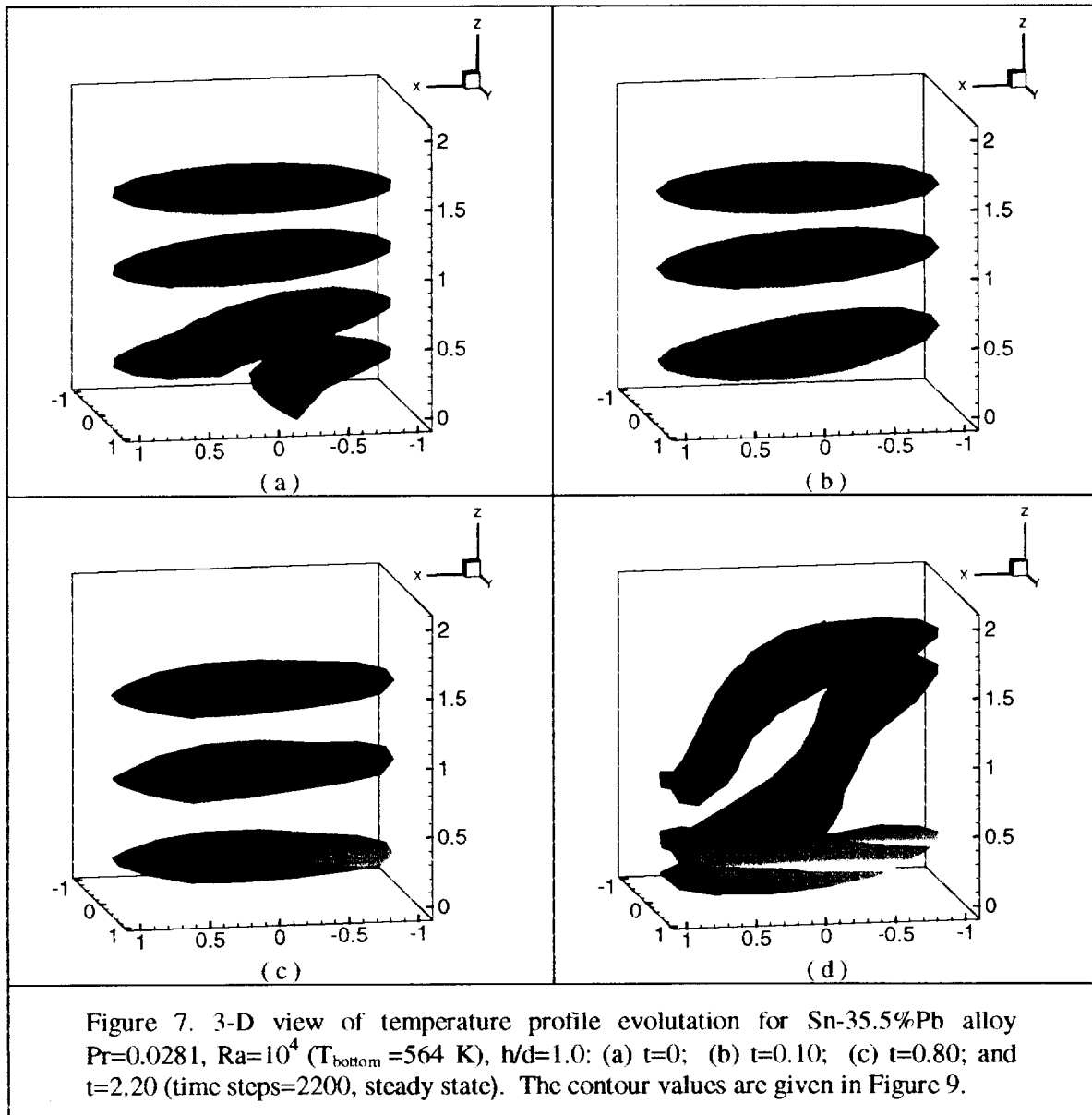


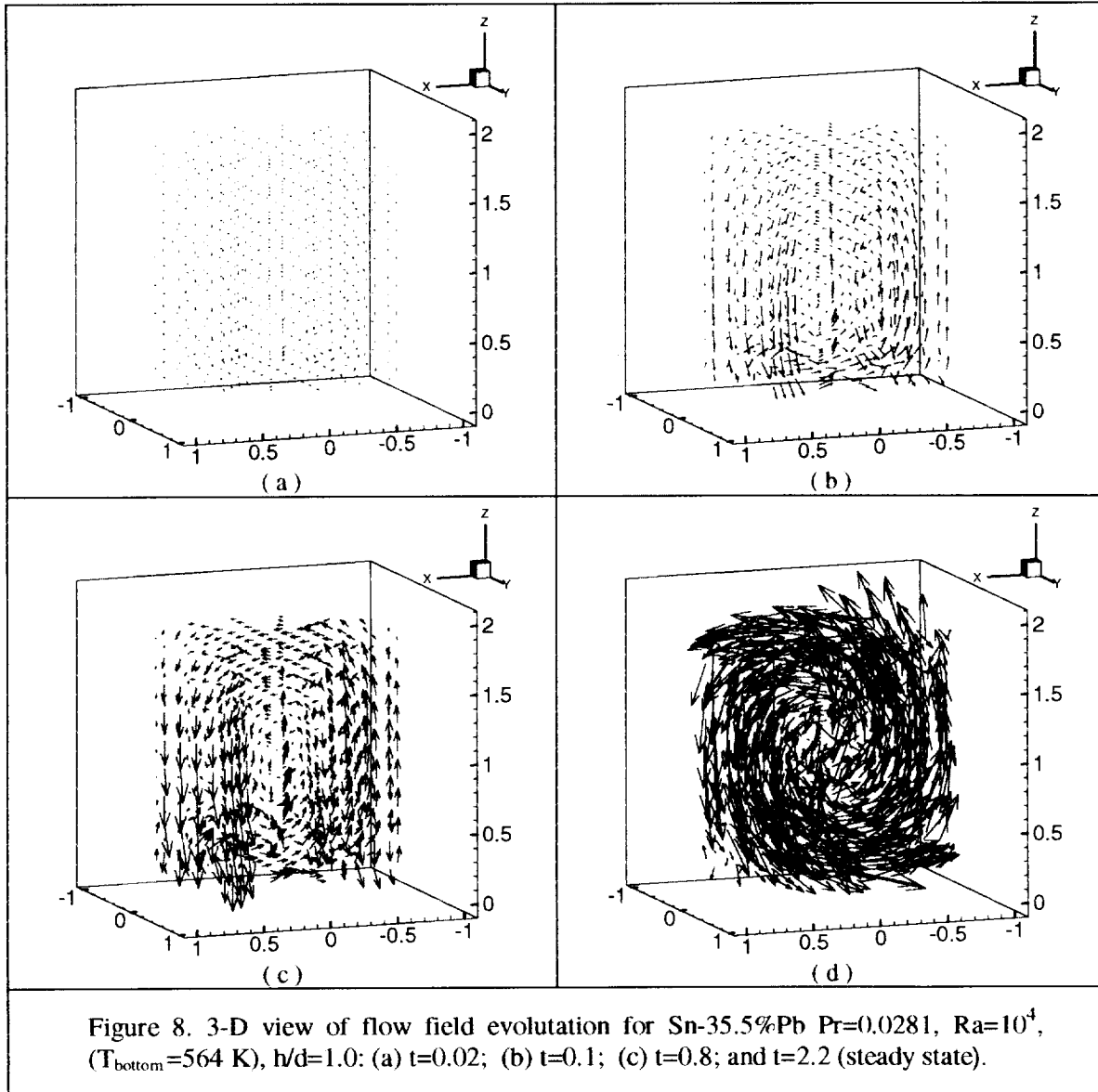


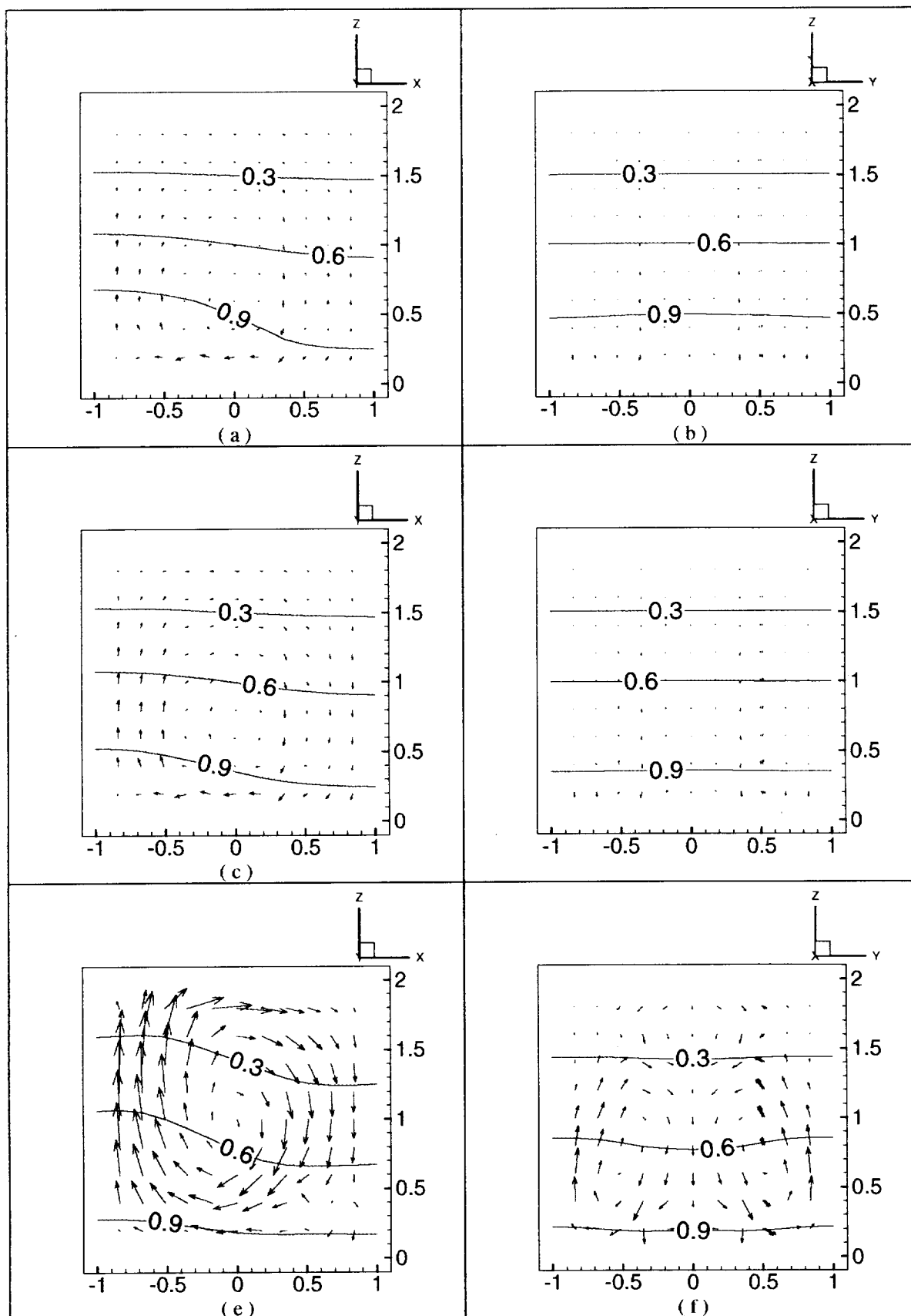


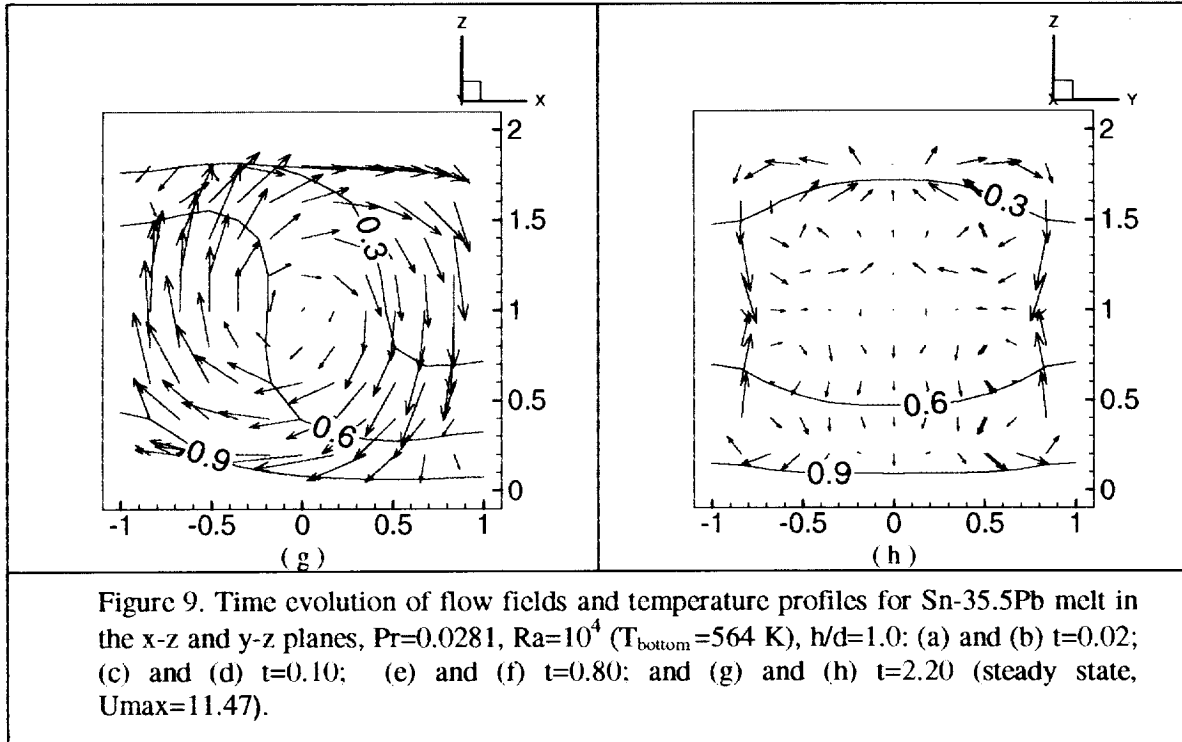












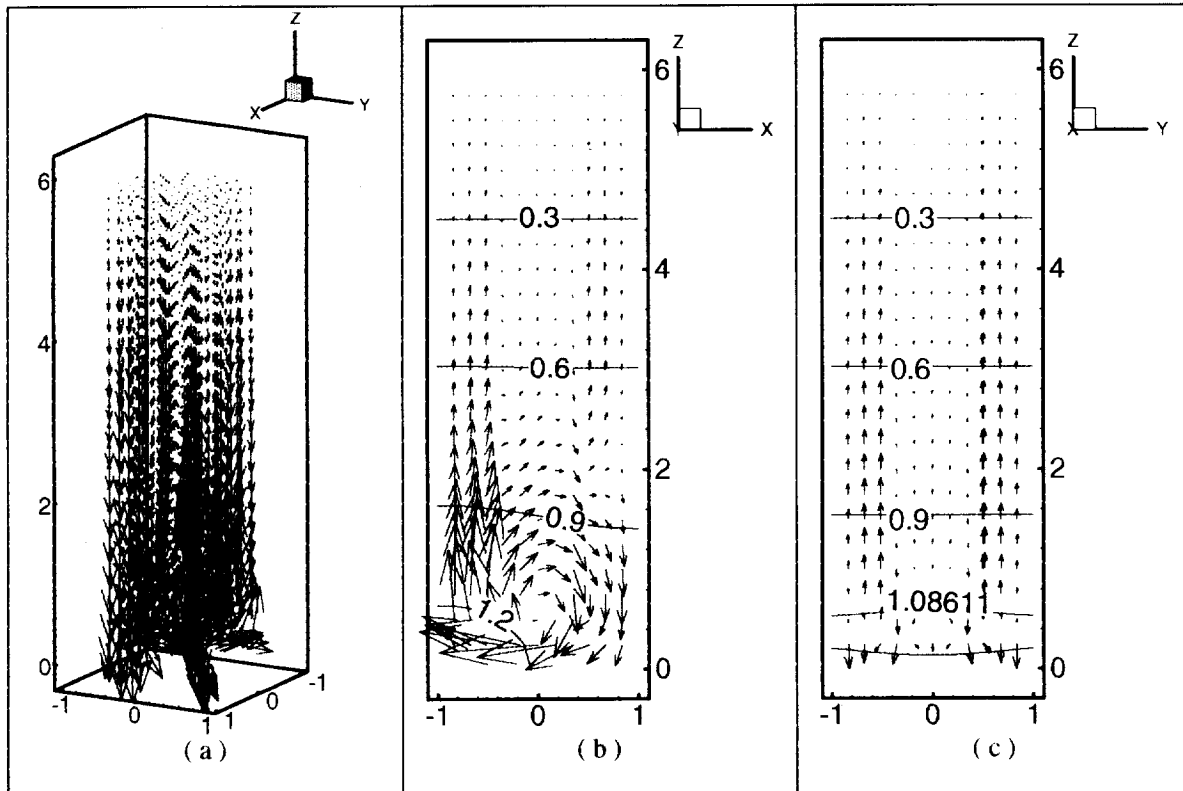
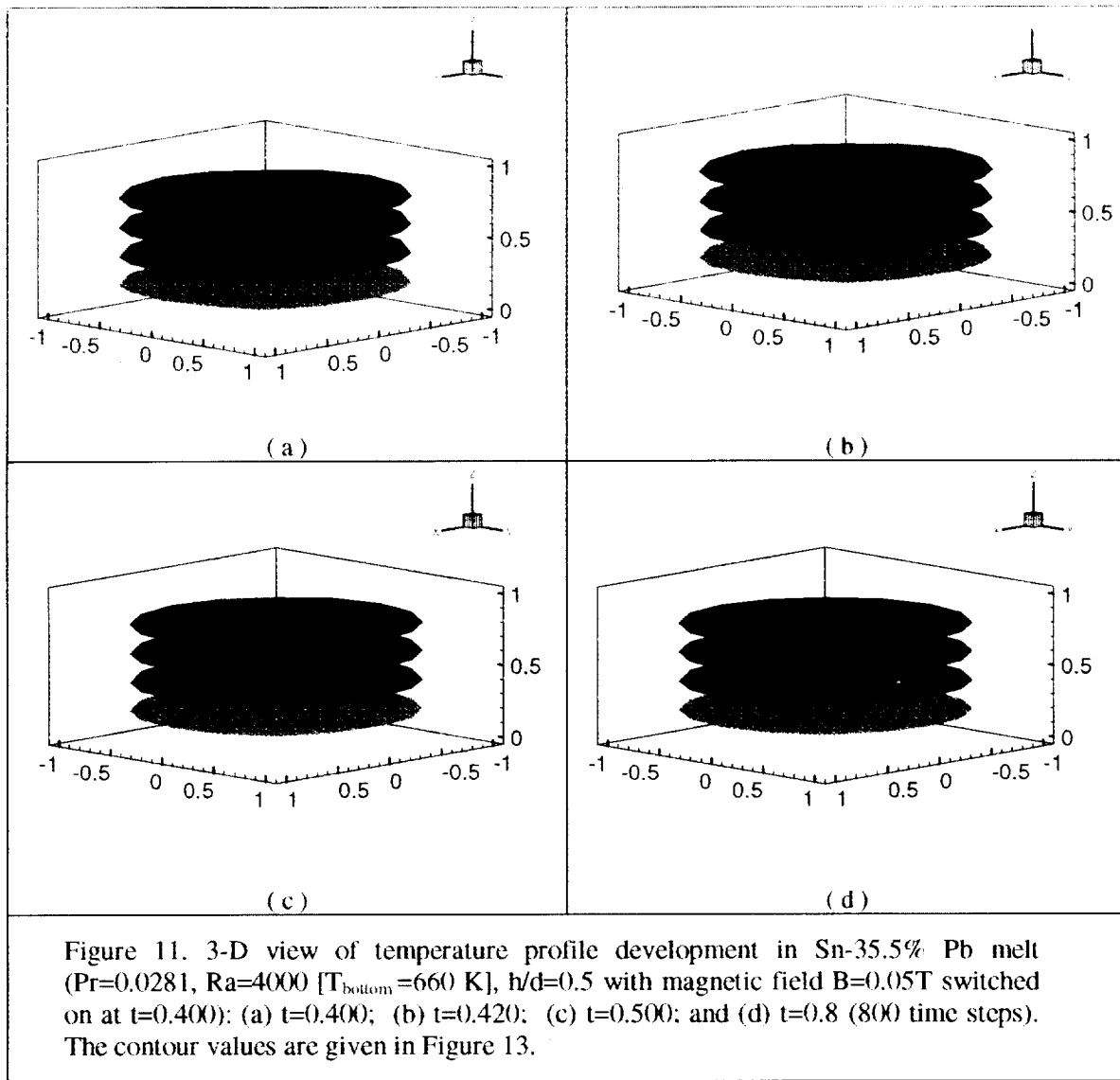
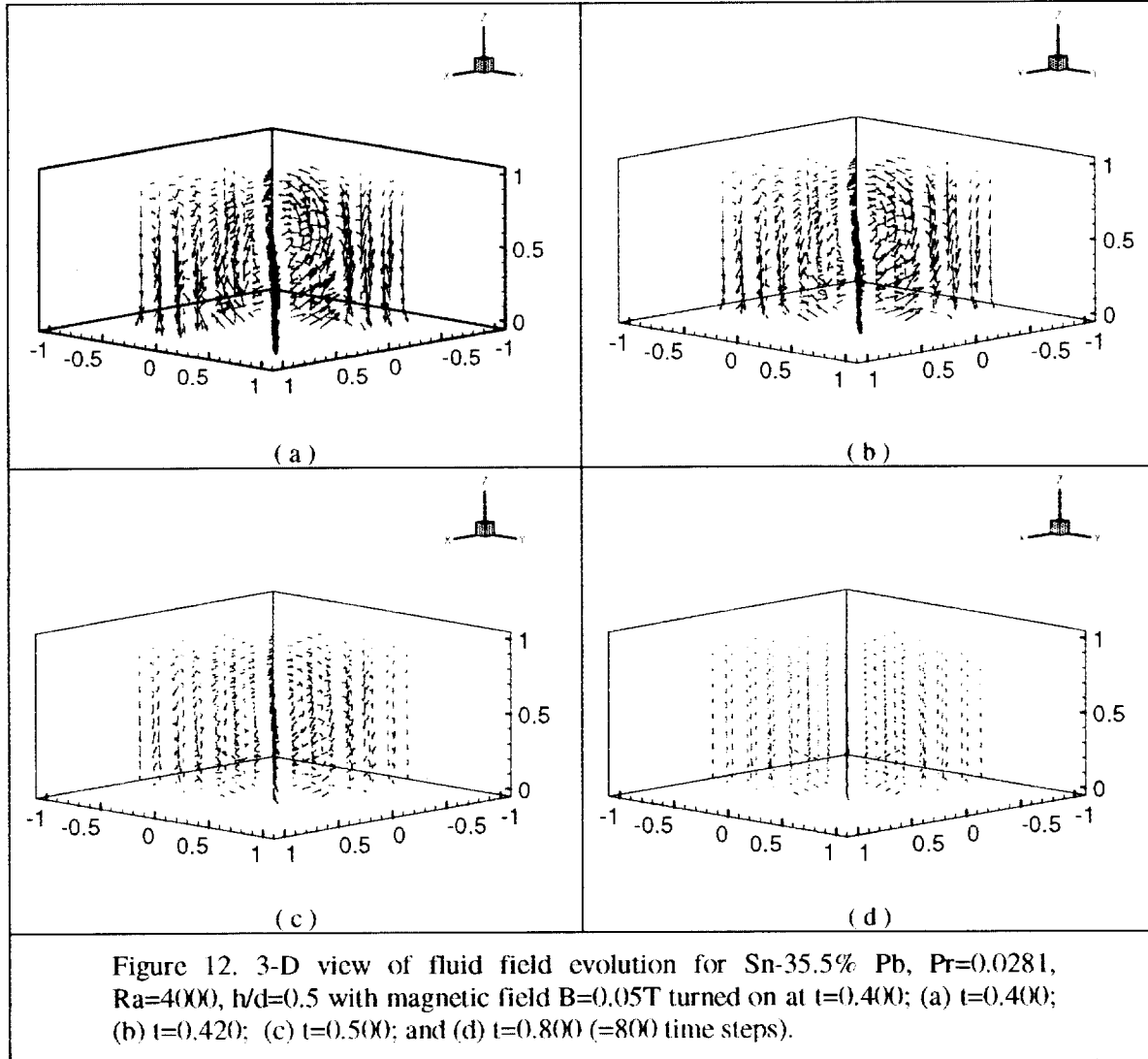


Figure 10. Fluid velocity and temperature profiles in the Sn-35.5% Pb melt, $Pr=0.0281$, $Ra=10^5$ ($T_{\text{bottom}} = 536$ K), $h/d=3.0$, (time steps=1100, steady state): (a) 3-D view of fluid field; (b) and (c) x-z and y-z plane cut views of flow pattern and temperature distribution. ($U_{\text{max}}=0.53$).





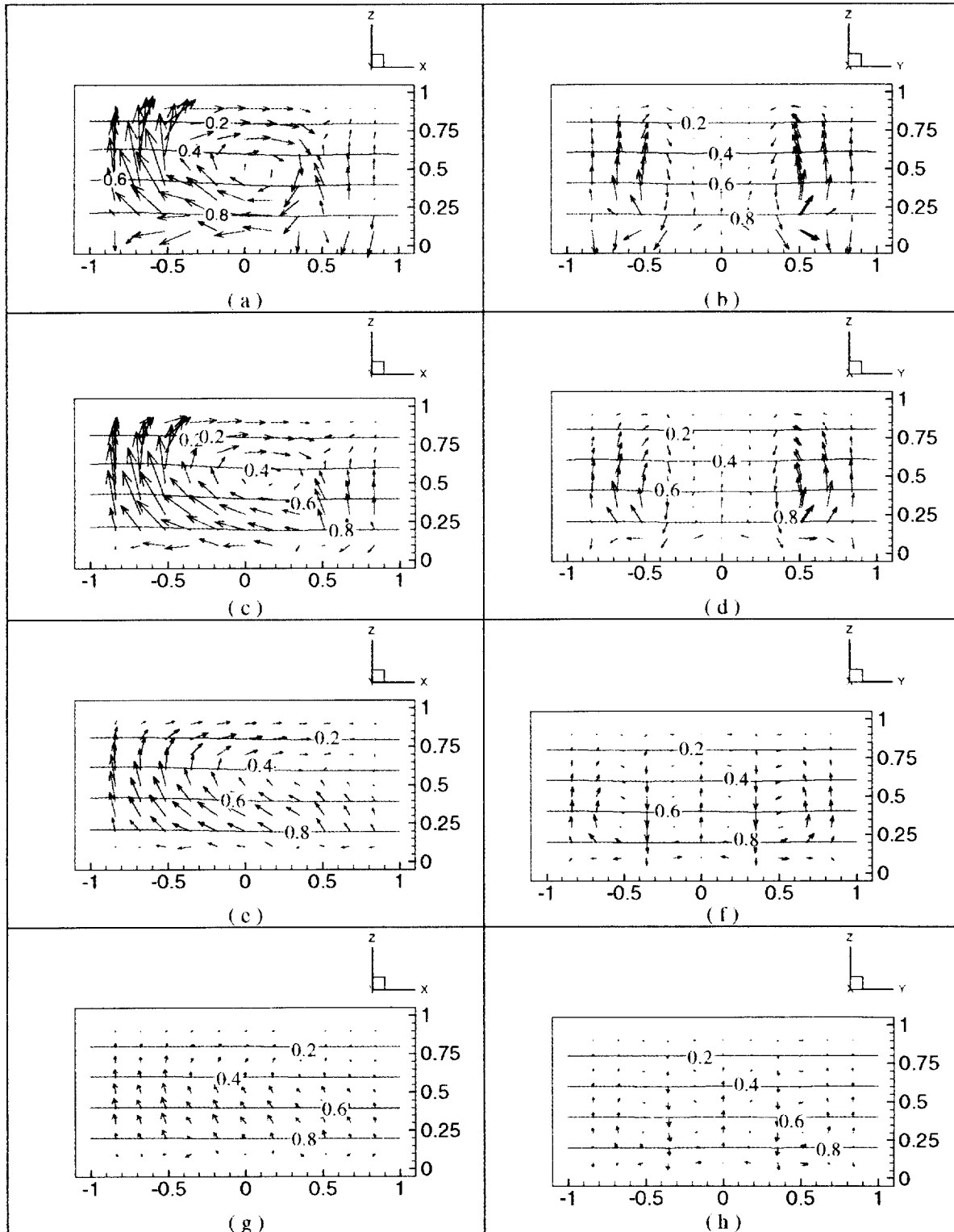
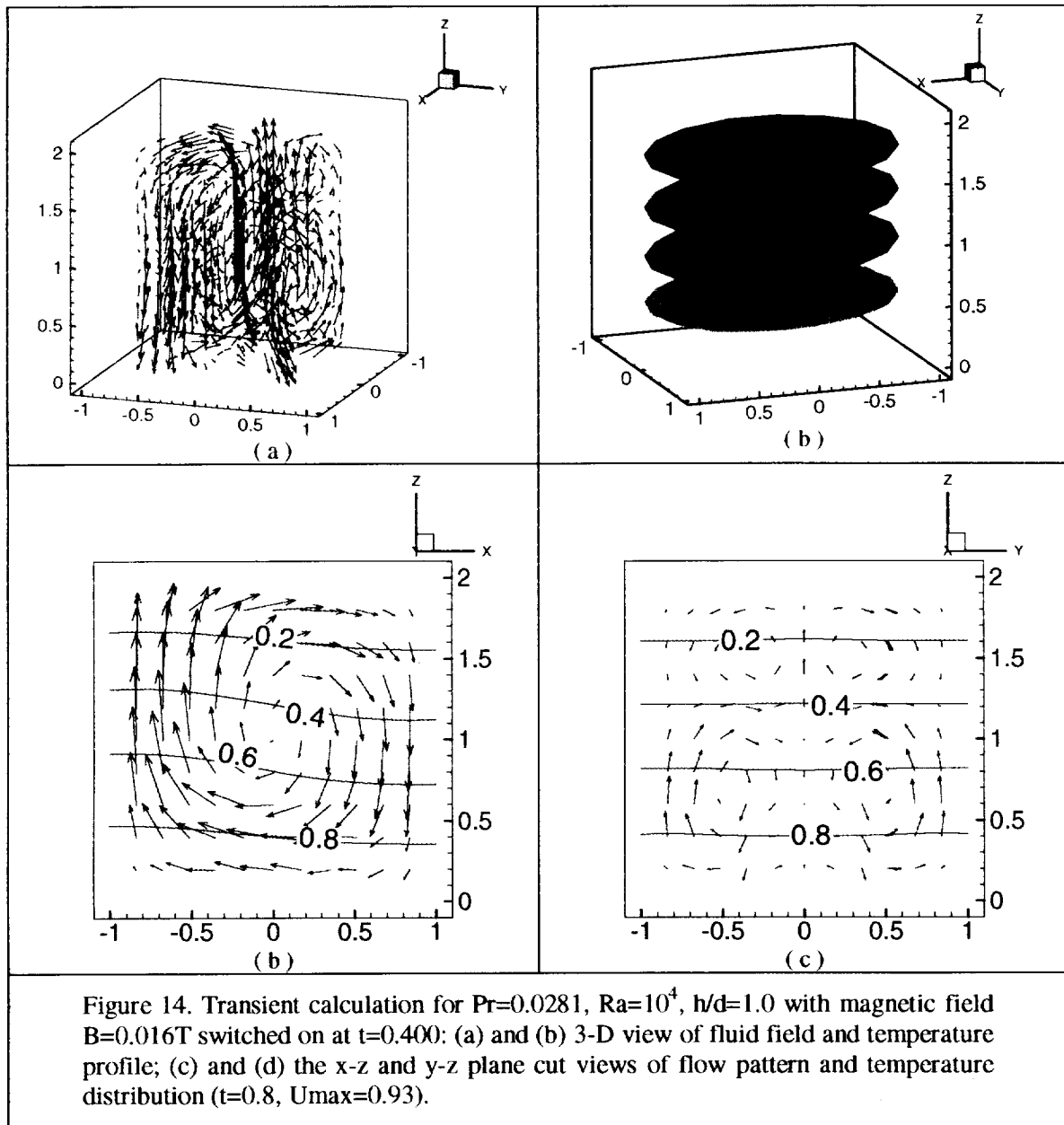
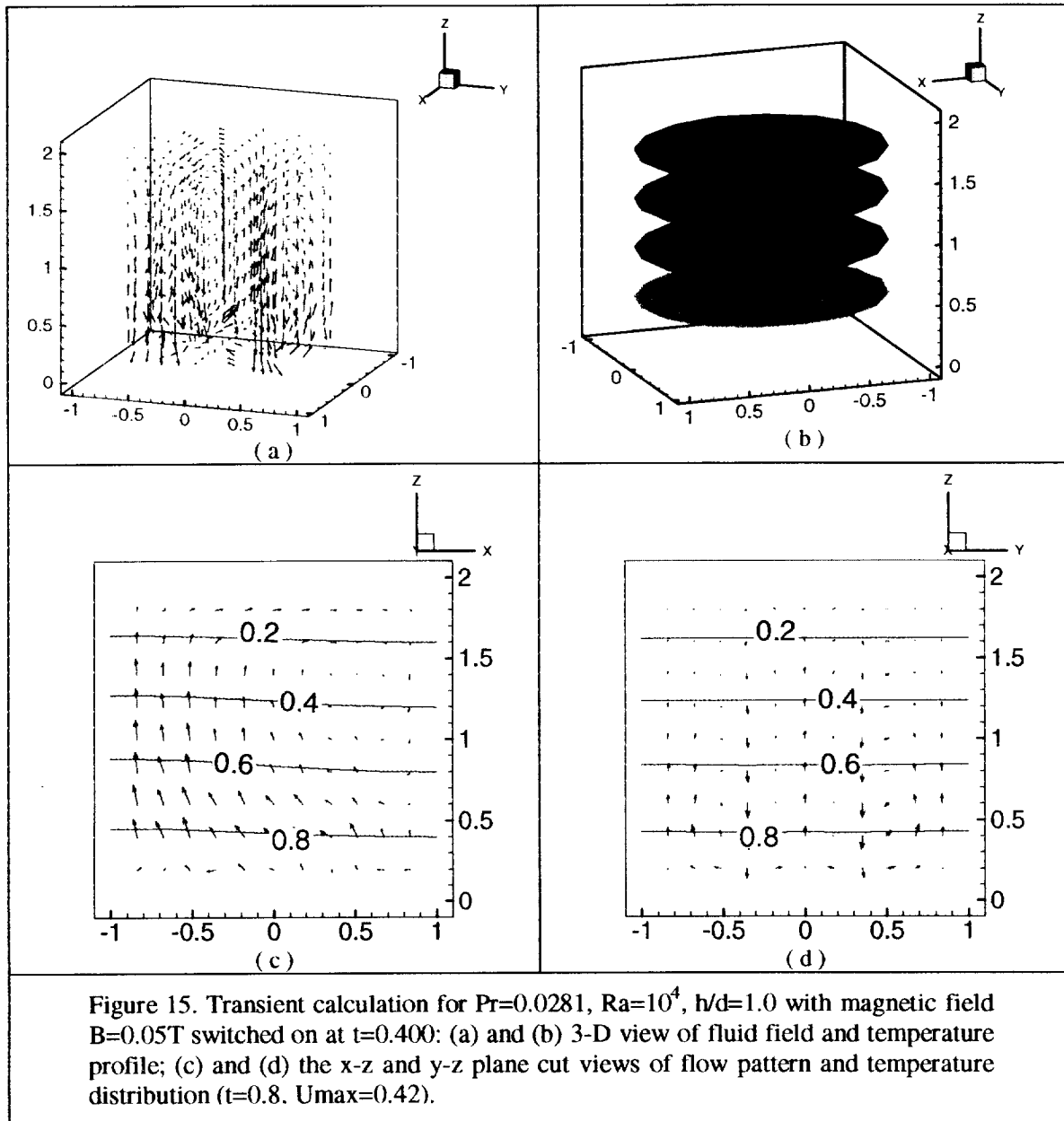


Figure 13. Transient development of flow fields and temperature profiles in the Sn-35.5% Pb melt, $Pr=0.0281$, $Ra=4000$, $h/d=0.5$ with magnetic field $B=0.05T$ applying at $t=0.4$; (a) and (b) $t=0.4$; (c) and (d) $t=0.420$; (e) and (f) $t=0.5$; and (g) and (h) $t=0.8$.





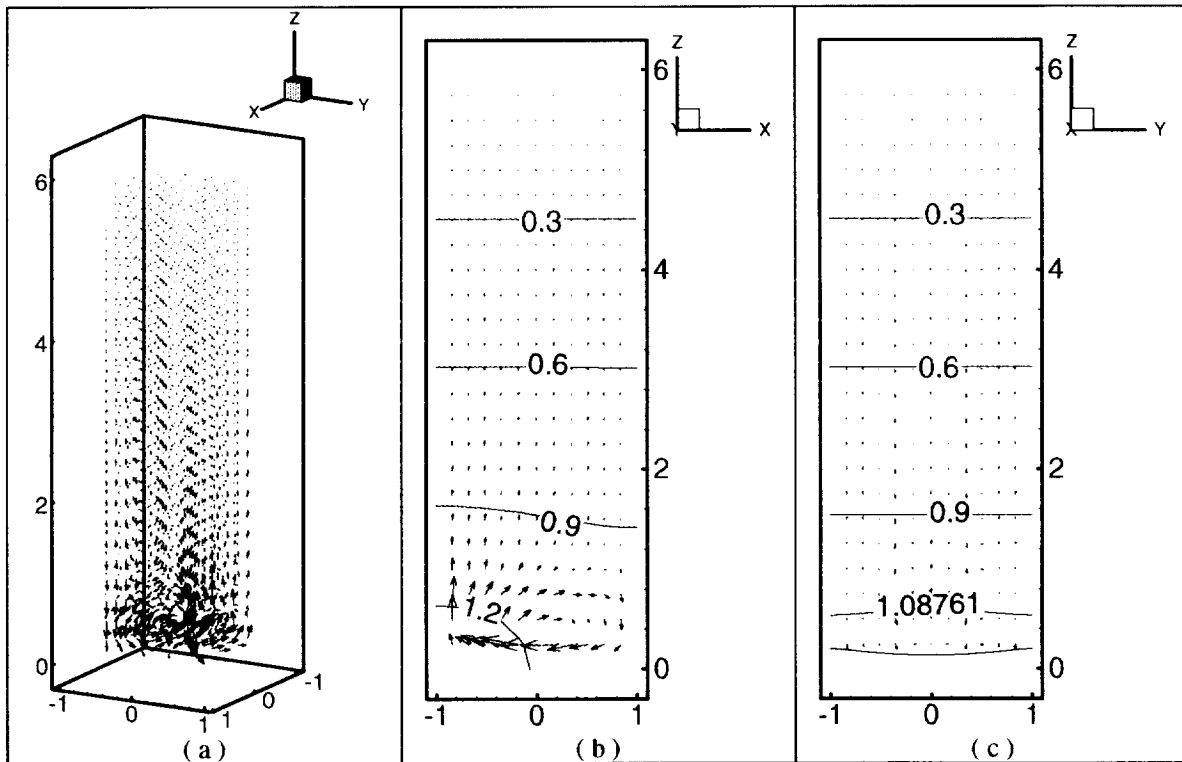
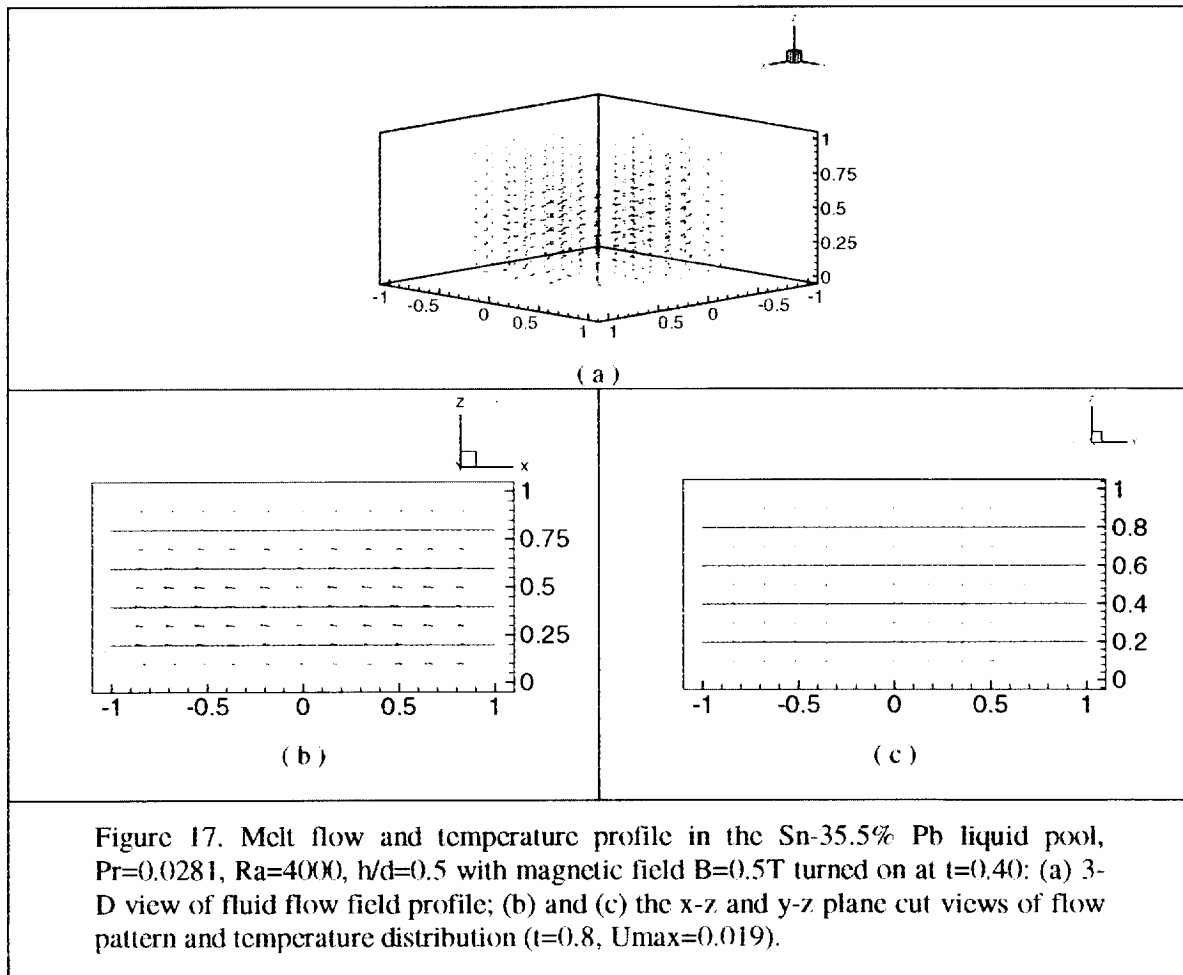
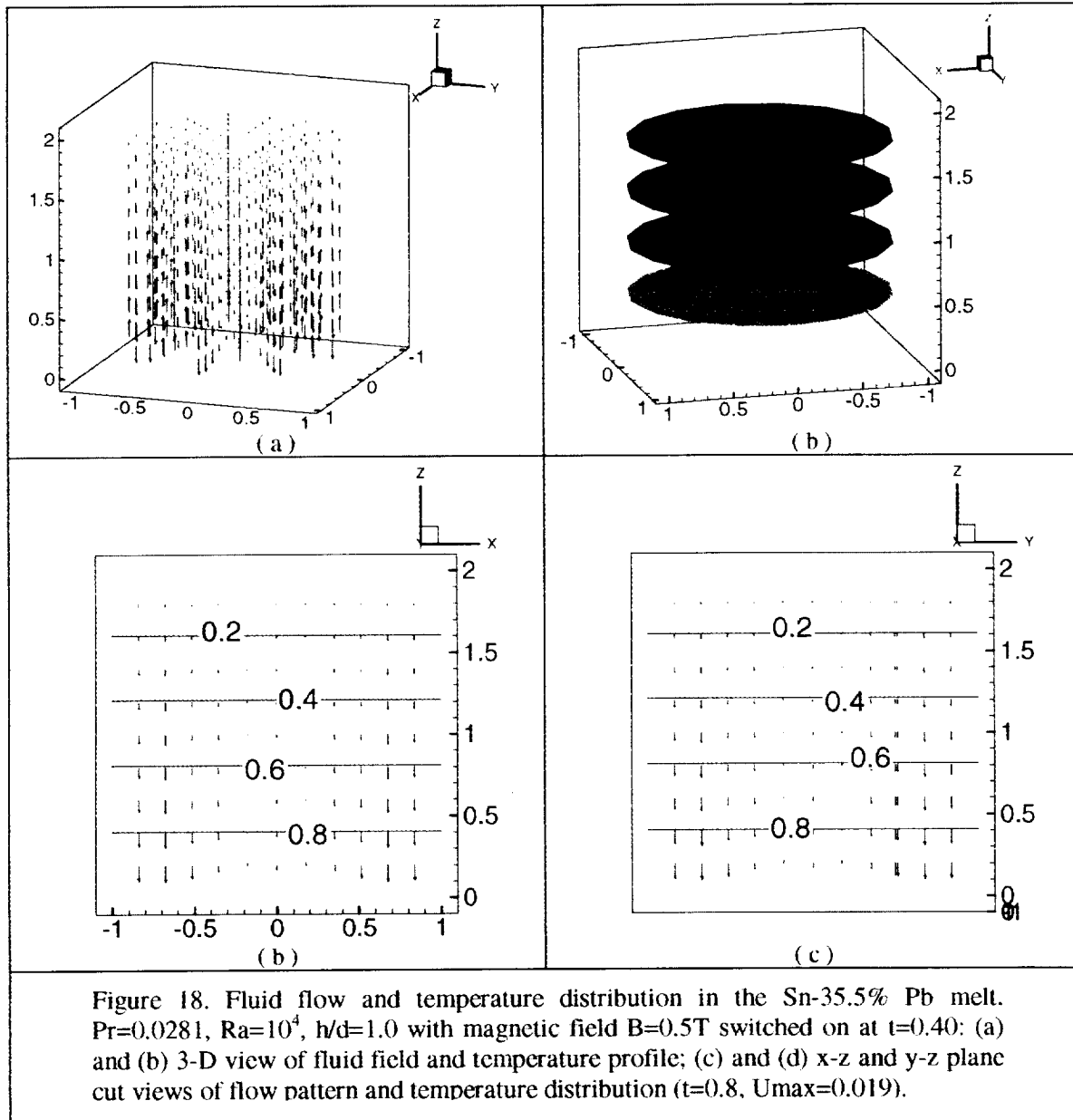
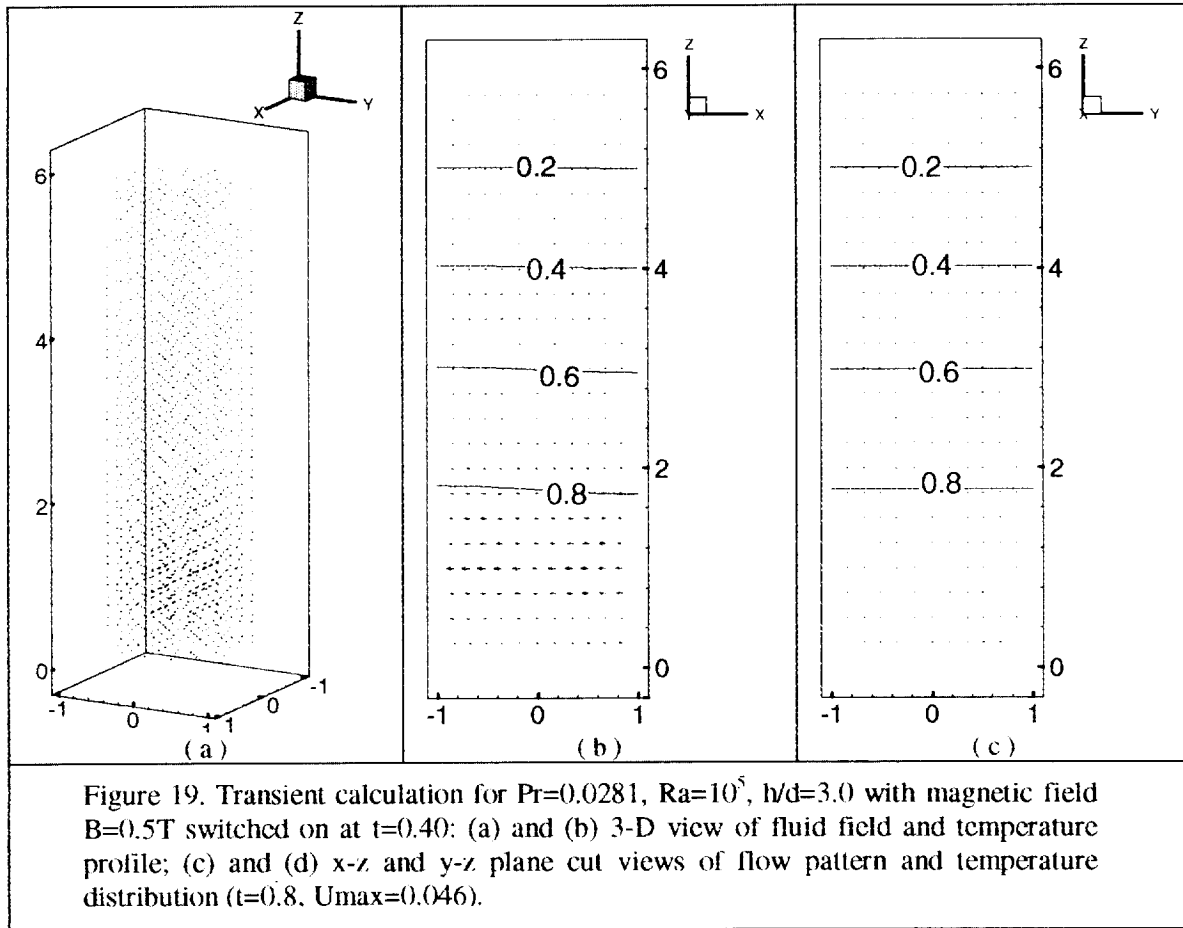
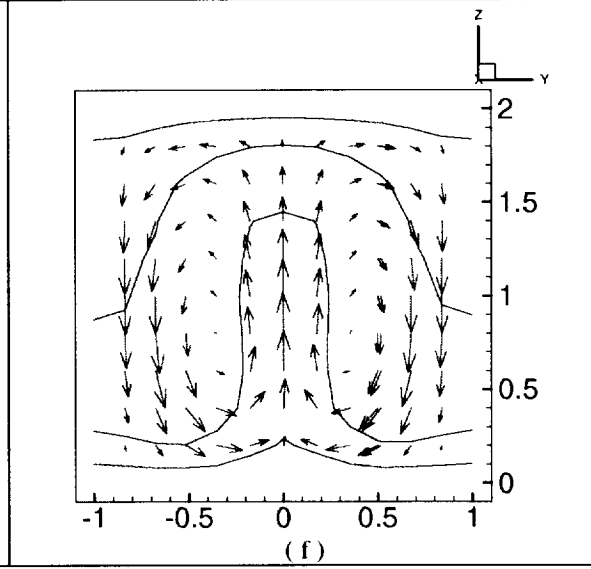
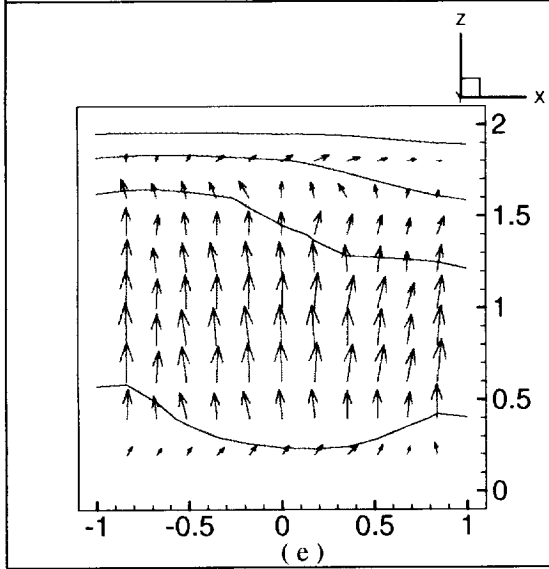
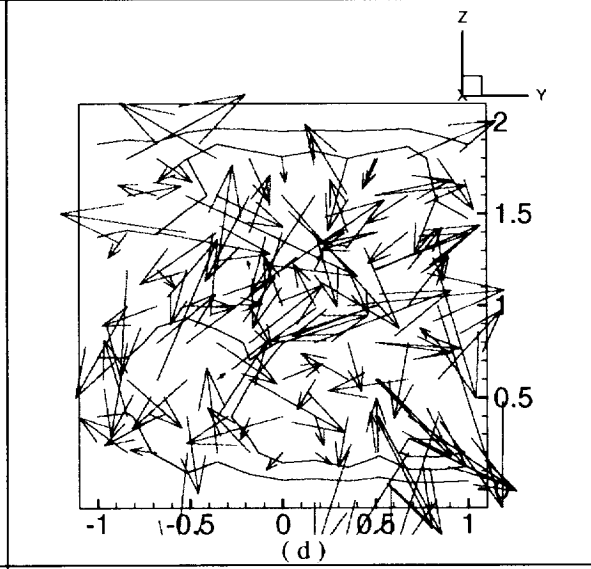
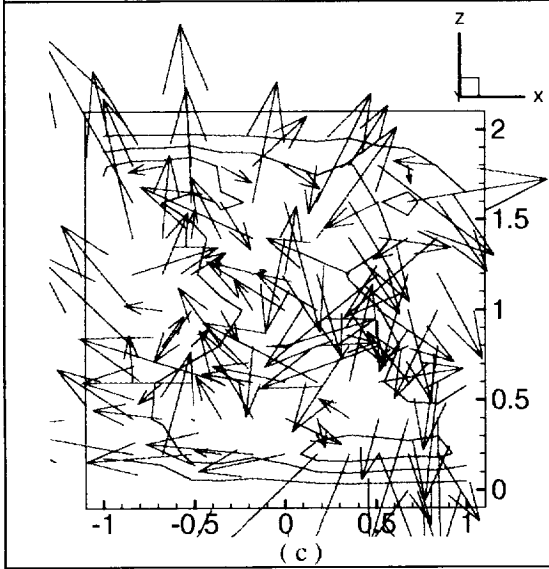
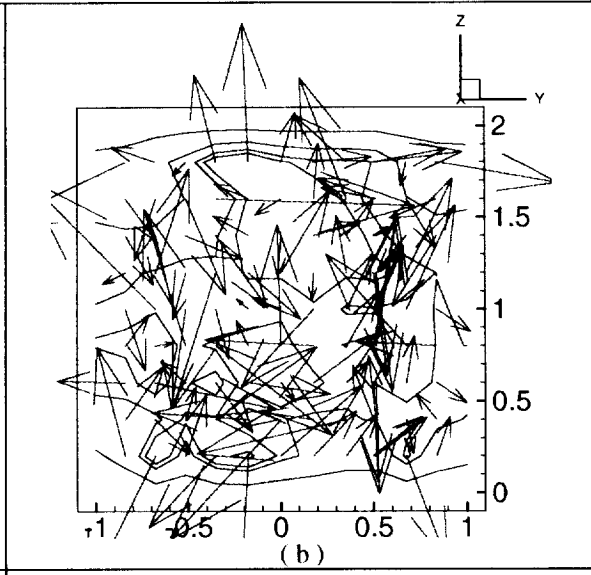
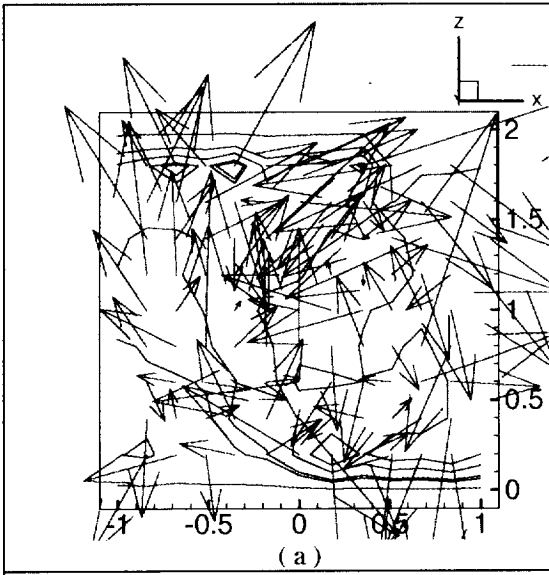


Figure 16. Velocity and temperature profile in the Sn-35.5% Pb melt, $Pr=0.0281$, $Ra=10^5$, $h/d=3.0$ with magnetic field $B=0.05T$ switched on at $t=0.4$: (a) 3-D view of fluid field; (b) and (c) x-z and y-z plane cut views of flow pattern and temperature distribution ($t=0.8$, $U_{max}=0.19$).









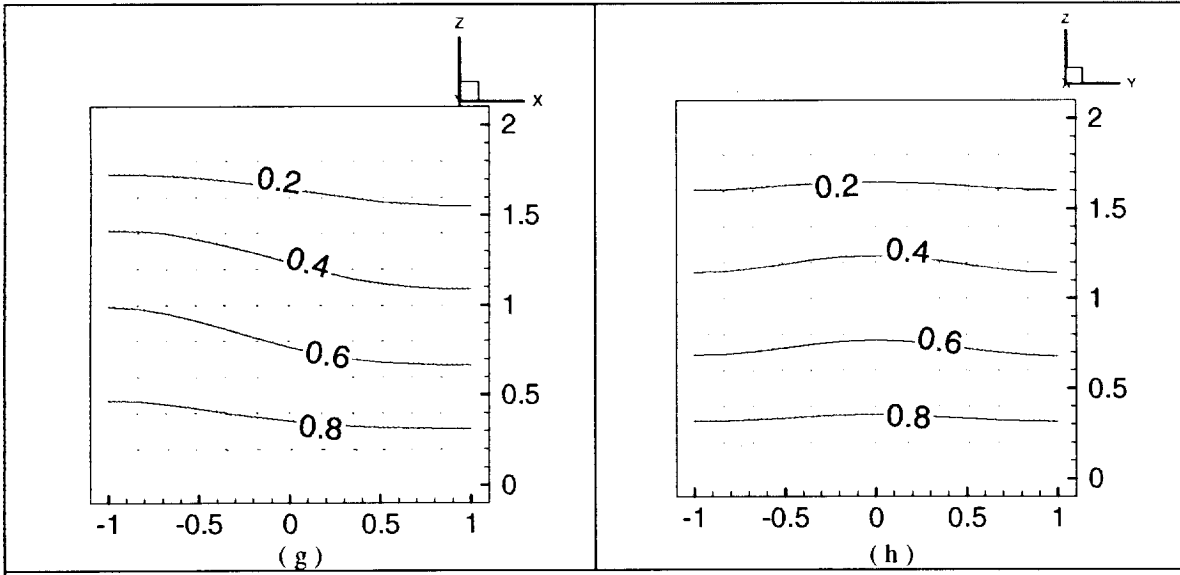


Figure 20. Dependency of the turbulent melt (Sn-35.5% Pb) flow on the applied magnetic field, $Pr=0.0281$, $Ra=8 \times 10^5$ ($T_{\text{bottom}}=4027$ K), $h/d=1.0$ with different magnetic field applying at $t=0.40$: (a) and (b) $B=0$, $U_{\text{max}}=172.50$; (c) and (d) $B=0.005\text{T}$, $U_{\text{max}}=96.59$; (e) and (f) $B=0.05\text{T}$, $U_{\text{max}}=38.79$; (g) and (h) $B=0.5\text{T}$, $U_{\text{max}}=1.57$, all at $t=0.8$.

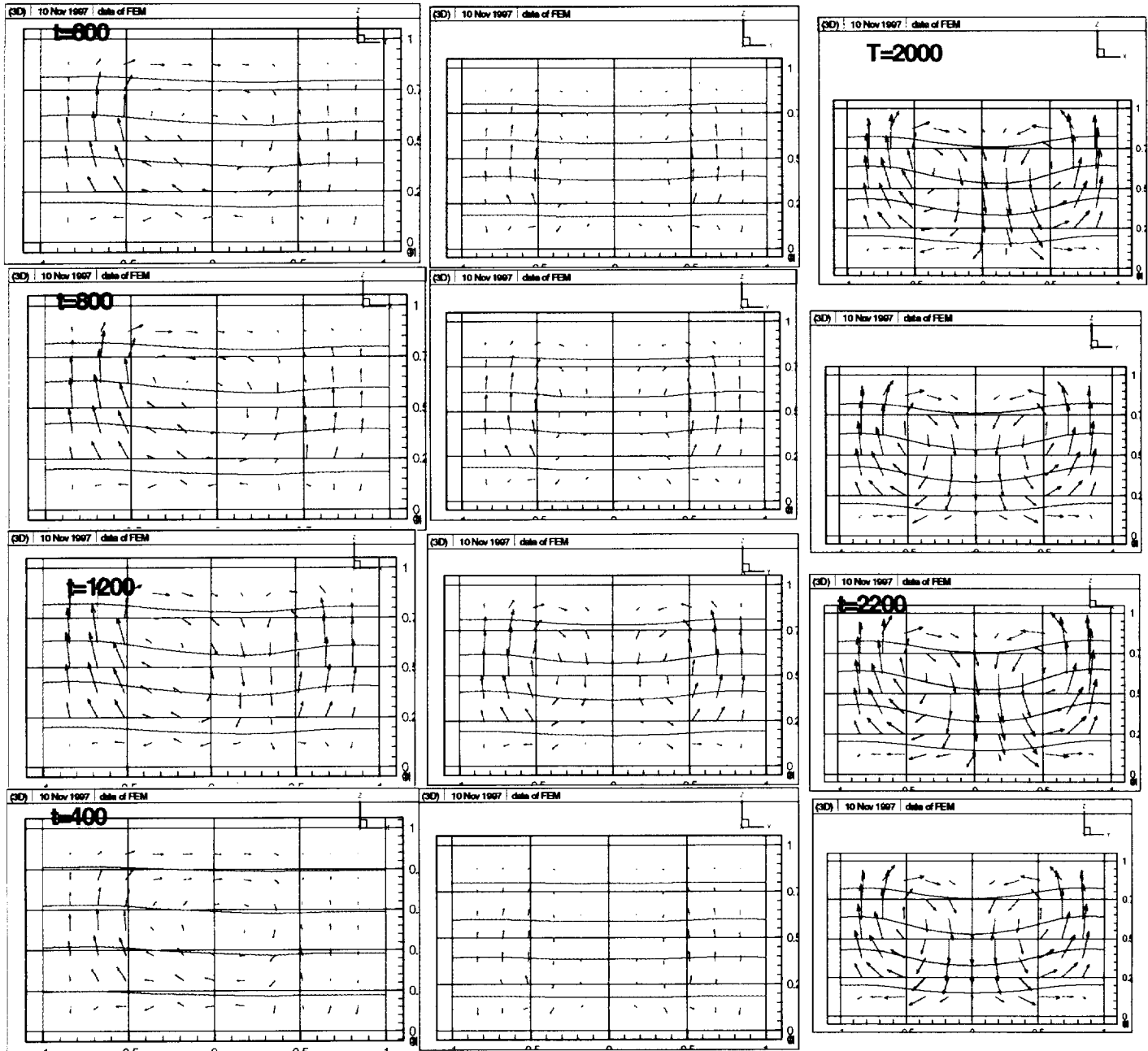
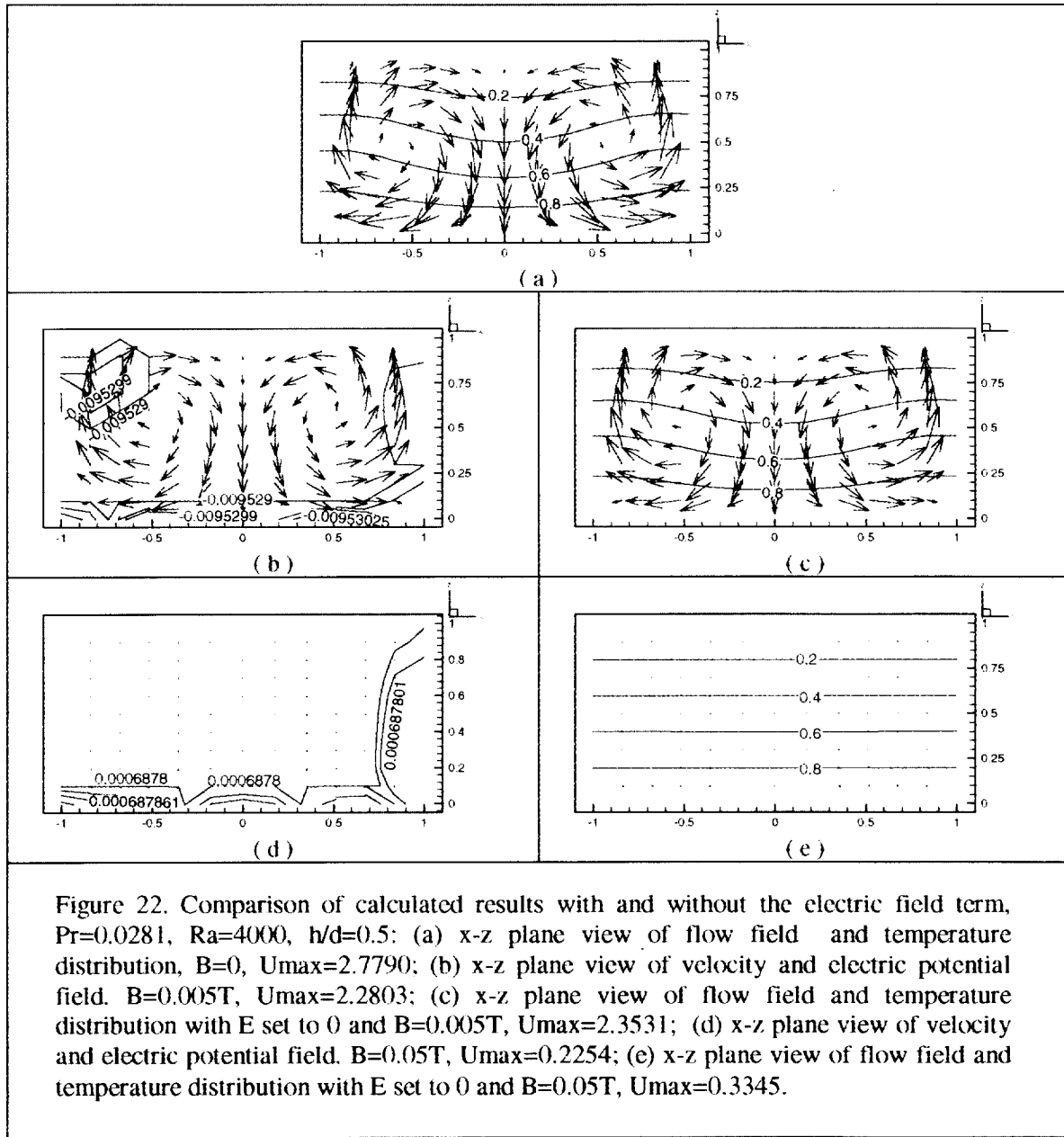


Figure 21. Fluid flow and temperature distribution in the Sn-35.5% Pb melt in 3-D cavity without the presence of an applied magnetic field. According to Muller's numerical simulations (run time (dimensionless) up to time steps=600), no symmetric flow patterns are possible. However, our calculations showed that if a longer time is used, a symmetric flow pattern starts to evolve and gradually attains a steady state. For the case shown, at time step=500, the computed results are similar to Muller's; and a steady state condition seems to be reached at time step=2400. The results here seem to suggest that additional work might be needed to further clarify some of the conclusions made in earlier studies by Muller's group (Muller 1988).



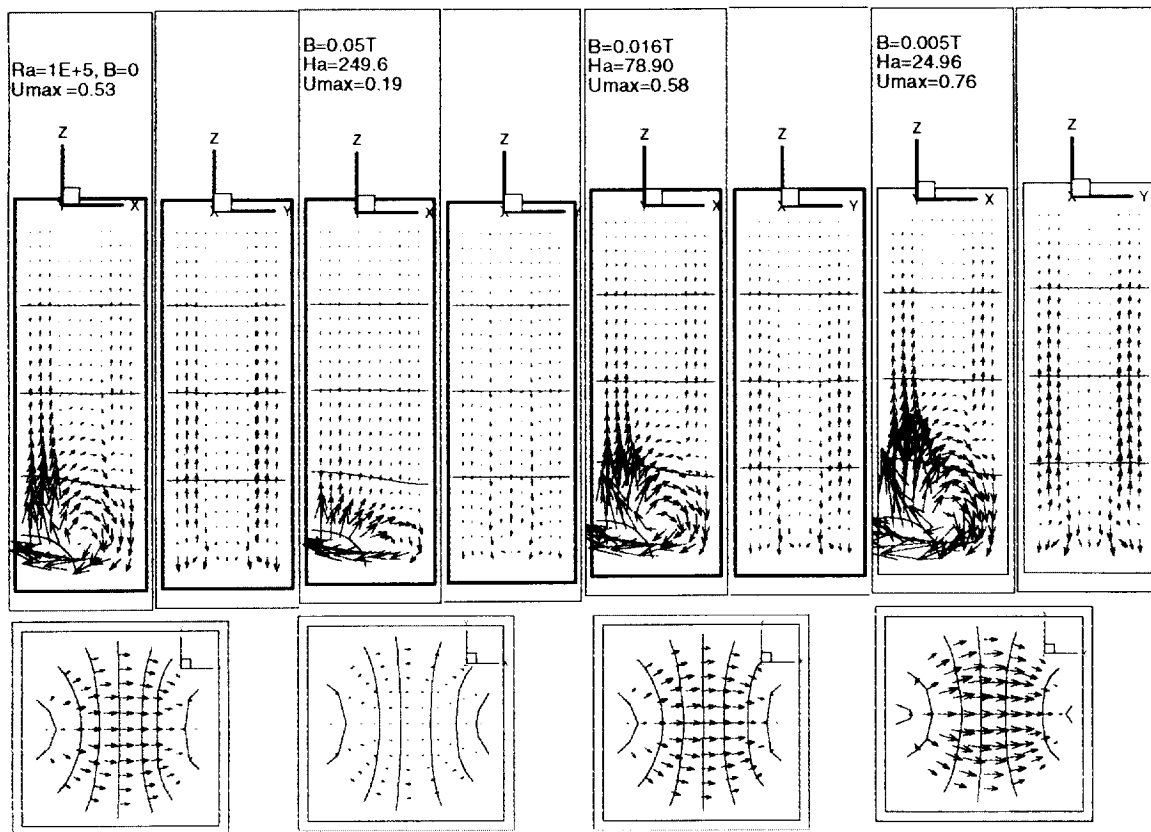


Figure 23. Dependency of the magnetic damping effects on the applied magnetic field strength. Note that with a weak magnetic field, the convection is actually enhanced. The threshold value of the applied magnetic field to achieve damping effects seems to be slightly larger than 0.016T.